THESIS FOR THE DEGREE OF DOCTOR OF PHILOSOPHY

# Mathematical Modelling of Cell Migration and Polarization

**Adam Malik**


CHALMERS
UNIVERSITY OF TECHNOLOGY

Department of Mathematical Sciences
Chalmers University of Technology
Gothenburg, Sweden 2020

Mathematical Modelling of Cell Migration and Polarization
Adam Malik
ISBN 978-91-7905-347-5



Doktorshavhandlingar vid Chalmers tekniska högskola
Ny serie nr 4814
ISSN 0346-718X

Department of Mathematical Sciences
Chalmers University of Technology and University of Gothenburg
SE-412 96 Göteborg
Sweden
Telephone: +46 (0)31 772 35 64

Typeset with LaTeX
Printed by Chalmers digitaltryck
Gothenburg, Sweden 2020

# Mathematical Modelling of Cell Migration and Polarization


## Adam Malik

Division of Applied Mathematics and Statistics
Department of Mathematical Sciences
Chalmers University of Technology



## Abstract

Cell migration plays a fundamental role in both development and disease. It is a complex process during which cells interact with one another and with their local environment. Mathematical modelling offers tools to investigate such processes and can give insights into the underlying biological details, and can also guide new experiments.

The first two papers of this thesis are concerned with modelling durotaxis, which is the phenomena where cells migrate preferentially up a stiffness gradient. Two distinct mechanisms which potentially drive durotaxis are investigated. One is based on the hypothesis that adhesion sites of migrating cells become reinforced and have a longer lifespan on stiffer substrates. The second mechanism is based on cells being able to generate traction forces, the magnitude of which depend on the stiffness of the substrate. We find that both mechanisms can indeed give rise to biased migration up a stiffness gradient. Our results encourages new experiments which could determine the importance of the two mechanisms in durotaxis.

The third paper is devoted to a population-level model of cancer cells in the brain of mice. The model incorporates diffusion tensor imaging data, which is used to guide the migration of the cells. Model simulations are compared to experimental data, and highlights the model's difficulty in producing irregular growth patterns observed in the experiments. As a consequence, the findings encourage further model development.

The fourth paper is concerned with modelling cell polarization, in the absence of environmental cues, referred to as spontaneous symmetry breaking. Polarization is an important part of cell migration, but also plays a role during division and differentiation. The model takes the form of a reaction-diffusion system in 3D and describes the spatio-temporal evolution of three forms of Cdc42 in the cell. The model is able to produce biologically relevant patterns, and numerical simulations show how model parameters influence key features such as pattern formation and time to polarization.

## List of appended papers

This thesis is based on the work contained in the following papers:

**Paper I: Malik, A.A.**, Gerlee, P. *Mathematical modelling of cell migration: Stiffness dependent jump rates result in durotaxis.*
in Journal of Mathematical Biology (2019)

**Paper II: Malik, A.A.**, Wennberg, B., Gerlee, P. *The impact of elastic deformations of the extracellular matrix on single cell migration: a mathematical framework.*
in Bulletin of Mathematical Biology (2020)

**Paper III: Malik, A.A.**, Rosén, E., Kundu, S., Krona, C., Nelander, S., Gerlee, P. *Modelling glioblastoma growth in a xenograft mouse model using diffusion tensor imaging*
Manuscript

**Paper IV:** Borgqvist, J., **Malik, A.A.**, Lundholm, C., Logg, A., Gerlee, P., Cvijovic, M. *Cell polarization in a bulk-surface model can be driven by both classic and non-classic Turing instability*
Submitted

## Author contributions

**Paper I:** I contributed substantially to model formulation, analysis, implementation of simulations and wrote the paper.

**Paper II:** I contributed substantially to model formulation, analysis, implementation of simulations and wrote the paper.

**Paper III:** I contributed substantially to model formulation, analysis, implementation of simulations and wrote the majority of the paper.

**Paper IV:** I made partial contributions to the derivation of the model, theoretical results and simulations, and to writing of the paper.

# Acknowledgements

I wish to express my deepest gratitude to my supervisor Philip Gerlee for constant support, always taking the time, for many good discussions about academic life, and for all the feedback on my work. I have learned incredibly much from you during these five years. I also wish to thank my co-supervisor Bernt Wennberg for many interesting mathematical discussions, and for all the good feedback on my work throughout the years. Thank you also to my examiner Torbjörn Lundh.

I want to pay my special regards to Marija Cvijovic. Your support and words of encouragement during these years have meant a lot to me. A dedicated thank you goes to Milo Viviani, with whom I shared my office. I have very much enjoyed our mathematical and non-mathematical discussions over these years.

Special thanks goes to the administrative staff of the department, for always being helpful and supportive. I wish to thank all my co-authors, in particular Johannes Borgqvist and Carl Lundholm.

I wish to acknowledge the superb working environment at the department, and I have all the colleagues and friends at the department to thank for that.

Finally I wish to thank my family and friends, and to dedicate this thesis to my cat Müsli, whom I love very much.

# Contents

# 1 Chapter I: Introduction

Mathematical biology, the use of mathematics to solve biological problems, is an enormous field of research to say the least. Although its history may not be as long or rich as mathematics in physics, mathematical biology nowadays utilizes tools from all major domains of mathematics and mathematical statistics. Upon opening a textbook such as *Essential Mathematical Biology* by Nicholas F. Britton from 2012 [10], one can read about how mathematics can be used in population dynamics, infectious disease, population genetics and evolution, biological motion, molecular and cell biology, pattern formation and tumor modelling. It is interesting to see that certain mathematical concepts span most, if not all, of the above fields of application.

An early example from the 13th century that could arguably be considered mathematical biology is Fibonacci's number sequence counting the number of rabbits in a growing population. Other major contributions to population dynamics were made by Malthus in the 18th and 19th century, and about a century later by Lotka and Volterra resulting in the well known predator-prey model.

Modelling the spread of infectious disease is a subject of great importance, and currently draws a lot of attention with the ongoing COVID-19 pandemic. An early example of such endeavors goes back to Bernoulli's work in 1760. He analysed the deaths from smallpox in an attempt to impact public policy to use variolation, i.e. injecting a mild strain of the virus to induce immunity [10]. However, the field only really took off in the early 1900's after Kermack and McKendrick [49] and other fellow contemporaries lay the foundation for the modern mathematical epidemiology.

Problems related to the growth and spread of tumors have been studied at least since the 1920's, with Hill studying the diffusion and consumption of oxygen [40], and Mayneord modelling the impact of radiation on the tumor growth in 1932 [61]. Since then the field has grown incredibly, and more sophisticated models have been developed.

Most of the classical fields of mathematical biology have been completely transformed by the recent technological development, most notably the increase in computational power, but also by more sophisticated techniques of microscopy, imaging and tissue engineering. Entire fields came into existence as the possibility to sequence DNA and proteins became a reality.

To visualize the growth of the field as a whole, and a few particular subfields, I used Google Scholar to search for articles containing specific keywords between the years of 1901 and 2020, divided into 6 intervals of 20 years du-

ration. The keywords chosen were required to occur anywhere in the article, and the number of articles found are plotted on the $y$-axis in a $\log_{10}$ scale and shown in Figure (1.1). Although the method used to collect the data is all but rigorous, and the analysis is coarse, it may be argued that these fields all have grown incredibly fast, even compared to the field of mathematics as a whole (in particular bioinformatics since the 1960's and onward).

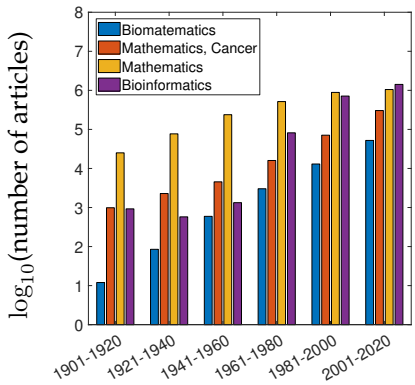


**Figure 1.1:** Number of search results obtained from Google Scholar for a number of keywords at different time periods. The $y$-axis shows the number of results found on a $\log_{10}$ scale.

When working in the field of mathematical biology one cannot escape to notice its connection to physics and the role that mathematics has played in its development. At the very least, certain theoretical frameworks have found their way to biology, for instance the tools developed in statistical mechanics which are now widely used in modelling the motion of cells and animals. This raises the question of whether there will ever be discoveries leading to universal laws in biology, comparable to those in physics. Although I am in no position to attempt to answer such a question (for interested readers see for example [77] and [22]) I will make an argument for the usefulness of mathematical modelling in biology, even if we should never find such universal laws.

The purpose of a mathematical model (compared to other models such as a conceptual-, visual-, or scale-models) is to very *precisely* describe a *subset* of reality. One needs to make decisions on what to include in the model and what to neglect. It follows that a model cannot be considered "real" or "true", rather, it should be useful in answering particular questions. The quote "Everything should be made as simple as possible, but not simpler", believed to have been uttered by Albert Einstein, does a good job at describing modelling. A too simple model is unlikely to capture complex phenomena, but too complicated models can suffer from issues of mathematical tractability or unreasonable computational demands. The process of modelling is often described as a cyclic process consisting of formulating a model, solving or simulating the model, and evaluating its ability to describe the data available. After having learned what it can or cannot do, modifications can be made to the model, and the process is

repeated.

Models which are not mathematical models are also used in experimental biology. An *in vitro* study of cell behaviour on an engineered surface, or the study of cells injected into a model organism such as a mouse are also examples of models of the more complicated system, for example the behaviour of the cells in the human body. As such they have limitations, however the purpose is to study a subset of reality, and hopefully be able to answer specific questions related to the original system.

Finally it should be emphasized that it is not only biology benefiting from the increased use of mathematics in biology. Attempting to solve complicated biological problems may very well give raise to new mathematical theories and techniques. A great example is the field of pattern formation, which was initiated by the seminal 1952 paper *The chemical basis of morphogenesis* by Alan Turing. Certainly many more such developments will be seen in the future, as the collaboration of the two fields develop further.

## 1.1 Thesis summary and statement of purpose

This thesis is concerned with mathematical modelling of cell migration and cell polarization. More specifically, the aim is to use modelling as a tool to further the understanding of the two topics of directed cell migration, and spontaneous symmetry breaking in cell polarization.

Leading up to the four papers is a biological background in Chapter 2, concerned with the relevance of cell migration in development and disease, how cell migration works, as well as cell polarization. Chapter 3 contains an overview of the mathematical tools related to the four papers. It begins with an overview of random walk models for cell migration, both with and without external bias. It then introduces the mathematical model used in **Papers I** and **II**, and discusses the strengths and weaknesses of both microscopic and macroscopic models. The last section is devoted to common modelling approaches in the field of cell polarization, and sets our model of polarization in its context. Chapter 4 contains a summary of each of the four papers contained in this thesis. Finally, Chapter 5 contains some concluding remarks.

The purpose of the introductory chapters is to provide the reader with the relevant background of the biological problems, as well as the mathematical tools, and to set the scene for, and put the papers in their proper context.

# 2 Chapter II: Biological background

Cell migration is the movement of cells from one location to another, often in response to chemical or mechanical cues from the environment. Both single cell and collective cell migration plays an essential role in both development and disease. The development of an embryo is dependent on the collective migration of cells, with different origins and target locations. Examples include cranial neural crest cells which originate in the head and neck and give rise to cartilage, bone and cranial neurons [53]. Trunk neural crest cells which start migrating from the back of the embryo contribute to the development of sympathetic neurons and pigment cells of the skin. These migratory events are highly complex and coordinated, and are believed to rely on cell-cell communication and interactions between individual cells and the chemical and mechanical properties of the local environment. Deviations or failures in the migratory events during development can have severe consequences including neurological disorders and heart disease. Cell migration also plays a key role during immune responses, when macrophages and neutrophils move to sites of infection, or when the migration of epidermal cells contribute to wound healing.

Although cell migration is clearly necessary for development and maintenance of individuals, it can also drive disease such as cancer. A characteristic property of cancer is the presence of abnormal cells which can divide uncontrollably and infiltrate surrounding tissues and organs. One of the hallmarks of malignant tumors is their ability to metastasize, that is, invade and proliferate at a secondary site, possibly far away from the location of the primary tumor [55]. During invasion, cells can migrate both as single cells or in collective formations such as sheets, or clusters [30], and are believed to have a range of migratory strategies and behaviour that help them overcome barriers during the invasion.

It is a well known fact that the local environment plays an important role in regulating cell behaviour, in particular the extracellular matrix (ECM), which is the non-cellular component present in all tissues and organs [29]. The ECM is mainly made up of water, proteins and polysaccharides, and offers a scaffolding for migrating cells. It is a dynamic structure that can be remodelled, either by being degraded by enzymes produced by cells, or by the forces generated by migrating cells. In section 2.1.1 we consider in greater detail various types of interactions between cells and the ECM, but first we take a look at how cell

migration works.

## 2.1 How cell migration works

There are two main means by which cells move, namely swimming and crawling. In animals, almost all cell movement is due to crawling, with the exception of swimming sperm. Swimming is possible for cells equipped with flagella, which are rigid helical structures that rotate to propel the cell forwards. Flagellated cells have been shown to move in a particular manner, by alternating between straight swimming and tumbling that reorients the cell [8].

The crawling type of movement is a complex and integrated process, resulting from interactions between the cell and its local environment. It is described as a cyclic process [78, 3] starting with polarization and extension of protrusions in the direction of migration, followed by attachment of the cell to the substrate and finally the generation of traction forces which cause the cell to move forward.

Cell polarization means that an asymmetry in molecular processes, shape or function is present within the cell, and the cell has a front and a back. The polarization process is highly complex and the establishment and maintenance of polarity is believed to be mediated by a set of feedback loops including Rho family GTPases, such as Cdc42. The formation and extension of protrusions are mainly driven by actin polymerization and can be thin spike-like actin bundles referred to as filopodia, or two-dimensional sheets consisting of a cross-linked mesh of actin filaments, which are referred to as lamellopodia. Some cells can also form three-dimensional protrusions filled with actin filament gel, called pseudopodia.

In order to pull itself forward the cell has to adhere to the extracellular matrix in which it is migrating, and does so using integrin receptors. The receptors act as the cell's feet and allow for adhesion to the substrate, and the formation of focal adhesions, which are the intra-cellular protein complexes that act as contact points between the cell and the surrounding matrix. The focal adhesions are believed to play an important role in the cell's ability to sense the mechanical properties of its environment [33, 81]. Once the leading edge of the cell is attached to the surrounding substrate, the cell can generate traction forces from myosin-based motors, which contract the intra-cellular actin fibers, and leads to the cell moving forward [56].

### 2.1.1 Directed migration and external bias

As a cell migrates through the ECM, it has the ability to sense its environment in a number of ways. One of the most well studied phenomena is chemotaxis which refers to the directed movement toward or away from chemicals and was discovered by Engelmann and Pfeffer [24, 72] in the 1880's. They observed that in a homogeneous environment with no external influence, swimming bacteria alternate between straight runs and tumbling to reorient, resulting in random motion. However, in the presence of a chemical gradient the frequency

of reorientation changes, which can result in a biased motion [94, 1]. Since then it has also been demonstrated that cancer cells exhibit chemotaxis [79], and that it can play a crucial role in tumor growth [18].

Another type of directed motion is haptotaxis, the name first put in print by Carter in 1965 [12]. Carter observed that mammalian cells cultured on cellulose acetate surfaces did not adhere properly, but when the surface was coated with metallic palladium they did adhere and spread. Experiments were conducted where an adhesion gradient was created in order to allow for varying degrees of adhesiveness, and the migrating cells showed a strong directional movement up the adhesiveness gradient. The role of haptotaxis in development and disease, including cancer [69], is still being researched.

A more recent discovery about the interplay between cells and its local environment was made in 2000 [58], when it was discovered that the rigidity, or stiffness, of the substrate on which cells are seeded influences the cell migration. In the original experiment, fibroblasts were seeded onto a flexible polyacrylamide sheet coated with collagen which was designed to have a discontinuity in rigidity resulting in a soft and a stiff region. When the cells were placed on the interface between the two regions, they showed a migratory preference for the stiff region. This phenomena is referred to as durotaxis, and has since been studied in a number of contexts, including cancer cell invasion. *In vitro* experiments of multiple glioma cell lines have demonstrated that both migration speeds and proliferation rates are significantly larger on stiff substrates [92], hinting at the importance of the mechanical properties of the ECM for cancer [23].

Durotaxis as well as the cell's ability to sense matrix stiffness are still not well understood, most likely because the observed phenomenon is the result of a large number of interacting mechanisms. Multiple studies have investigated how the absolute stiffness and the stiffness gradient influence durotaxis. It has been shown that the durotactic response is mostly dependent on the gradient strength, and less so on the absolute stiffness [44, 23, 93, 47]. This has been demonstrated in terms of both increased velocity as well as the magnitude of bias in the motility. One hypothesis explaining this is due to the reinforcement of adhesion sites on stiff regions. When focal adhesions are subjected to repeated tugging by the cell, the focal adhesions located in stiffer regions may become reinforced as a result, increasing their lifetime [73, 31]. This hypothesis is investigated in a mathematical model and is presented in **Paper I**, where it is assumed that the average lifetime of focal adhesions depend on the local stiffness of the substrate.

In the original article first describing the phenomena, possible mechanisms explaining the behaviour were discussed. Among them was one which states that if an elastic band is stretched across a gradient of rigidity, the mass distribution becomes skewed towards the stiff side. A cell which repeatedly exerts forces large enough to deform the substrate of unequal amounts in different regions may in the long run tend to move more toward the stiff side. However, the authors disregard this, on the basis that the displacements caused by the cells are too small. This mechanism is investigated in **Paper II**, where we developed a mathematical model based on the assumption that cells are able

to deform the substrate, and investigate if this mechanism could result in a migratory bias towards stiffer regions on the substrate.

Durotaxis can be studied on a wide range of scales, from the sub-cellular level to the population level. It is believed that the focal adhesions play a key role in rigidity sensing, and that the underlying mechanism involves a force-dependent stretching of proteins, which recruits other signaling molecules [38, 33], but the details remain elusive. One can also zoom out and focus on the behaviour at the single-cell scale, and in doing so a number of general features have been discovered. It appears that cells are able to generate larger traction forces on stiff substrates [80, 39, 11], and that their spreading area also increase with stiffness. With an increase in spreading area, the average force of each focal adhesion decreases [39], but the total force over all adhesions increases. The precise relationship between the traction force, spread area and stiffness are not fully understood, but the analysis in [39] suggests that stiffness influences traction forces directly and does not require spreading.

### 2.1.2 Cell migration and cancer

Understanding the mechanisms governing cell migration is important for diseases such as cancer. Two of the hallmarks of cancer are invasion and mestastasis, i.e. the formation of a secondary tumor. Cancer cells can migrate either as single cells or in collective formations, and can sometimes change their migratory behavior in response to changes in their environment, including drug therapy [30]. An example of a particularly aggressive form of brain cancer is glioblastoma, with a dismal prognosis of survival of approximately one year after diagnosis [5, 41]. One of the difficulties with surgical removal is that the cancer cells migrate large distances, resulting in diffuse tumors. As a consequence tumor recurrence is seen in 95% of the cases [34].

The brain tissue is typically divided into grey matter and white matter. Grey matter contains cell bodies, glial cells, axons, dendrites, and blood vessels [28], while the white matter contains mostly myelinated axons, giving it a white appearance. Studies have shown that glioblastoma cells tend to migrate along white matter tracts and blood vessels [34, 26]. This motivates research into how the brain anatomy may influence the spread of cancer cells in the brain. Sophisticated imaging techniques such as diffusion tensor imaging (DTI) is now being incorporated into mathematical models of tumor growth [86]. This is the subject of **Paper III**, where we develop a mathematical model of migrating cells, in which DTI data is incorporated into the model.

## 2.2 Cell polarization

We previously mentioned that polarization is an important step in cell migration. Polarization is in fact essential to many other processes in biology including differentiation and proliferation, and occurs in both single-cell organisms such as budding yeast, but also in multicellular organisms [27]. The enzyme Cdc42, which is a small GTPase of the Rho family, found in all eu-

karyotic cells is believed to play an essential role in polarization [27, 7]. Cdc42 can be GTP-bound (Guanosine triphosphate) referred to as its active form, or GDP-bound (Guanosine diphosphate) and is then said to be in its inactive form. The name active comes from "signaling-active", referring to the GTP-bound form's ability to propagate signals [7]. Polarization occurs as GTP-bound Cdc42 accumulates locally at the membrane, and contributes to cytoskeletal changes [15]. In budding yeast for example, the aggregation of Cdc42 precedes budding events during which it divides. The localized accumulation can be induced by spatial cues such as cell-cell contact and soluble factors [27], but can also occur spontaneously in the absence of any spatial cues, referred to as spontaneous symmetry-breaking [95, 48, 60].

The cycling between the two states is promoted by GEFs (Guanine nucleotide exchange factors) and GAPs (GTAPase-activating proteins), where GEFs promote activation and GEFs inactivation. Apart from the GTP-bound and GDP-bound forms, residing close to the plasma membrane, Cdc42 can also bind to GDI (guanine nucleotide dissociation inhibitors) keeping it in an inactive form and retaining it in the cytosol of the cell. In addition to the activation-inactivation mediated by GEFs and GAPs, it is believed that complexes are formed by PAKs (p21-activated kinases), various scaffold proteins and GEFs, which diffuse freely in the cytoplasm [15]. Active GTP-bound Cdc42 recruits these complexes from the cytoplasm to promote further activation of neighbouring Cdc42. Figure 2.1 illustrates the relationship between the different forms of Cdc42 and the other key players.

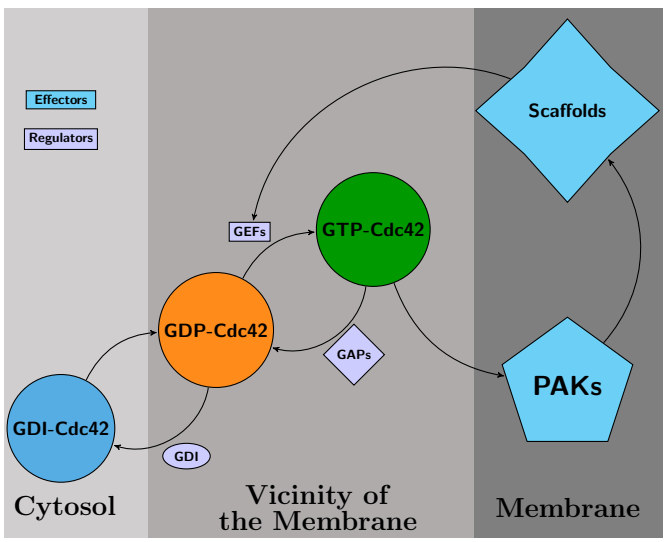


**Figure 2.1:** Schematic illustration of the activation and inactivation of Cdc42.

When this highly complex process is translated into mathematical terms, it results in a model that tracks the concentrations of GTP-, GDP-, and GDI-bound Cdc42, along with the choice of functions that govern the conversion of one

form to the others. This is illustrated in Figure 2.2. As the phenomena of interest is spatio-temporal in nature, the most common models take the form of reaction-diffusion equations (see [46] for a comparison of mathematical models used to model polarization). For some time it has been discussed whether spontaneous symmetry breaking could be the result of a Turing-type mechanism [37]. That is the phenomena where, under certain conditions, chemicals can react and diffuse and produce steady state heterogeneous spatial patterns [65]. This is the topic of **Paper IV**, where we investigate the possibility of a mathematical model to produce patterns of relevance in the context of polarization. This will be discussed in greater detail in Section 3.5.

The problem of spontaneous symmetry breaking we have modelled in **Paper IV** is more relevant in the case of budding yeast, or more generally, where spatial cues are not driving the polarization process. However, Cdc42 plays an important role also during polarization of migrating cells [43, 27]. In this context though, it is likely more relevant to study polarization in connection to soluble factors and environmental cues.

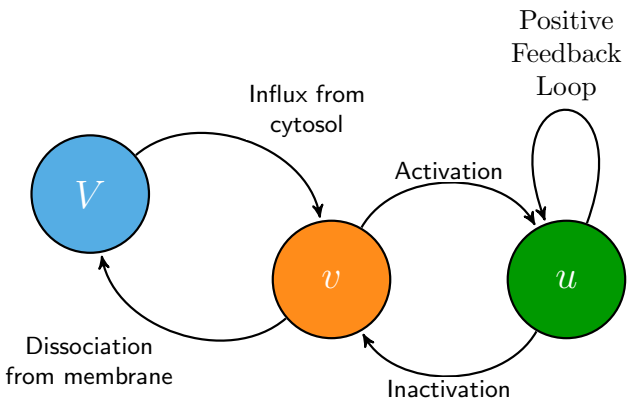


**Figure 2.2:** Schematic illustration of the activation and inactivation of Cdc42. The GTP-, GDP- and GDI-bound forms of Cdc42 are denoted by $u$, $v$ and $V$ respectively.

# 3 Chapter III: Mathematical background

In this chapter we begin by introducing a number of mathematical models, or frameworks, used to model cell migration. We begin by describing the most simple random walk in section 3.1, as well as the correlated random walk. Section 3.2 is devoted to external bias in the random walk, which is commonly used to model directed motion of cells. In Section 3.3 we present an alternative model of cell migration which we used in **Papers I** and **II**, and also highlight the strengths and weaknesses of microscopic and macroscopic models in Section 3.4. Finally we discuss models of cell polarization and set our model in its proper context in Section 3.5.

## 3.1 Random walks

We begin by describing the simplest possible random walk, and then proceed to make it more general and increase its complexity, and discuss how these additions can be motivated by biologically observed phenomena.

The most simple type of random walk is the one-dimensional random walk on the integers, where the agent (also referred to as walker, individual, or particle) starting at the origin performs random jumps to one of the two neighbouring sites, with a fixed time between jumps, denoted $\Delta t$. Each jump is random and the probability of moving left or right is $q = 1/2$, and each jump is independent of both the current position and the previous jump. This type of random walk is discrete in time and space, and it is unbiased because the probability of moving left or right is equal. For such a process, one can ask the following question [13, 66]: What is the probability, $p(m, N)$, that after $N$ such jumps the particle is located at position $m \in \mathbb{Z}$? Because of independence, all sequences of $N$ jumps are equally likely, and all occur with probability $(1/2)^N$. The random walker ends up at position $m$ if a total of $(N + m)/2$ is taken in the positive direction, and $(N - m)/2$ in the negative direction. There are a total of $\binom{N}{\frac{N-m}{2}}$ ways this can happen, resulting in the probability

$$p(m, N) = \left(\frac{1}{2}\right)^N \binom{N}{\frac{N-m}{2}},$$

which, for large $N$ and $m \ll N$ can be approximated using Stirling's formula, to result in

$$p(m, N) \approx \sqrt{\frac{2}{\pi N}} e^{-\frac{m^2}{2N}}.$$

When $N$ is large it is convenient to introduce a more general step length $\Delta x$, so that the position of the walker is given by $x = m\Delta x$. Similarly, denote by $\lambda$ the rate at which steps are taken, and write $N = \lambda t$, and let

$$P(x, t)dx = p\left(\frac{x}{\Delta x}, \lambda t\right) \frac{dx}{2\Delta x},$$

where $P(x, t)dx$ is the probability that the walker finds itself between $x$ and $x + dx$. Then we have

$$P(x, t)dx = \frac{1}{\sqrt{2\pi\lambda\Delta x^2 t}} e^{-\frac{x^2}{2\lambda\Delta x^2 t}} dx.$$

By letting $\lambda \to \infty$ and $\Delta x \to 0$ in such a way that the limit $\lambda\Delta x^2 = 2D$ is constant, we obtain

$$P(x, t) = \frac{1}{4\pi D t} e^{-\frac{x^2}{4Dt}}.$$

Here it can be noted that $P$ is the fundamental solution to the diffusion equation

$$\begin{aligned} &\frac{\partial P}{\partial t} = D\frac{\partial^2 P}{\partial x^2}, \text{ for } x \in \mathbb{R}, t > 0, \\ &P(x, 0) = \delta(x), \end{aligned}$$

where $\delta(x)$ is the Dirac distribution. We can see that as the rate of jumps increase to infinity, and the length of jumps decreases to 0, while maintaining the requirement that $\lambda\Delta x^2 = 2D$ is constant, the jump-process is a diffusion process. The solution to the diffusion equation gives the probability density function for the position of the unbiased random walker starting at the origin.

We next consider the slightly more general case, where the probability of moving to the right is $0 \leq q \leq 1$ and the probability of moving to the left is $1 - q$. We illustrate an alternative way to go from the discrete random walk to a continuous description of the probability density $P(x, t)$ for the location of the random walker taking steps of size $\Delta x$ once every $\Delta t$ units of time. Now we consider the master equation approach [16], which is an alternative way of deriving an equation for $P$, by writing down the expression for $P$ at a future time $t + \Delta t$:

$$P(x, t + \Delta t) = qP(x - \Delta x, t) + (1 - q)P(x + \Delta x, t). \tag{3.1}$$

The two terms on the right hand side describe the two possible ways in which a walker can end up at position $x$ at time $t + \Delta t$. It can either have been located at the neighbouring site to the left, $x - \Delta x$, and moved to the right with probability $q$. Alternatively, it may have been located at $x + \Delta x$, and moved left with probability $(1 - q)$. To proceed we have to assume that the parameters

$\Delta x$ and $\Delta t$ are small, and that we can expand the terms using their Taylor expansions

$$P(x,t+\Delta t) = P(x,t) + \Delta t \frac{\partial P}{\partial t}(x,t) + \frac{\Delta t^2}{2}\frac{\partial^2 P}{\partial t^2}(x,t) + \mathcal{O}(\Delta t^3),$$
$$P(x-\Delta x,t) = P(x,t) - \Delta x \frac{\partial P}{\partial x}(x,t) + \frac{\Delta x^2}{2}\frac{\partial^2 P}{\partial x^2}(x,t) + \mathcal{O}(\Delta x^3),$$
$$P(x+\Delta x,t) = P(x,t) + \Delta x \frac{\partial P}{\partial x}(x,t) + \frac{\Delta x^2}{2}\frac{\partial^2 P}{\partial x^2}(x,t) + \mathcal{O}(\Delta x^3).$$

Inserting these expressions into Equation (3.1) and simplifying, we obtain

$$\frac{\partial P}{\partial t} = \frac{\Delta x}{\Delta t}(1-2q)\frac{\partial P}{\partial x} + \frac{\Delta x^2}{2\Delta t}\frac{\partial^2 P}{\partial x^2} + \mathcal{O}(\Delta x^3) + \mathcal{O}(\Delta t^3). \tag{3.2}$$

One can now study different limiting cases as $\Delta x, \Delta t \to 0$ as well as the case $q \to 1/2$ [16], which can be done in multiple ways.

We first consider the case where $(\Delta x/\Delta t) \to \alpha$, which implies that $(\Delta x^2/\Delta t) \to 0$. This results in Equation 3.2 becoming

$$\frac{\partial P}{\partial t} = \alpha(1-2q)\frac{\partial P}{\partial x},$$

which is referred to as a simple transport equation.

Another choice comes from $(\Delta x^2/\Delta t) \to 2D$, which was described previously for the unbiased random walk. We can now consider two different cases for $q$. First, if $q = 1/2$, corresponding to the unbiased case seen previously, then we obtain pure diffusion

$$\frac{\partial P}{\partial t} = D\frac{\partial^2 P}{\partial x^2}. \tag{3.3}$$

However, we can also consider the case where $q \to 1/2$, in such a way that $(\Delta x/\Delta t)(1-2q) \to c$. This choice of scaling results in an advection-diffusion equation:

$$\frac{\partial P}{\partial t} = c\frac{\partial P}{\partial x} + D\frac{\partial^2 P}{\partial x^2}.$$

We clearly see how we can obtain equations which are drift dominated or diffusion dominated, depending on the choice of scaling.

This type of random walk model can be used as a starting point to model the movement of cells. In the case where a large number of cells are modelled, the continuous model may be more suitable.

### 3.1.1 Continuous time and space

A more general way to model random motion is through the continuous-time random walk (CTRW), where the waiting time between jumps is a random variable, $T_i$, and the jump size is a random variable $R_i$ (possibly continuous) [63, 52]. A random walker starting at $R_0 = 0$ at time $T_0 = 0$ makes its first jump of random length $R_1$ after waiting a time $T_1$, and a random jump $R_2$ after

time $T_2$, and so on. It is often assumed that the pair $(R_i, T_i)$ is independent of preceding and succeeding pairs, but the jump $R_i$ may depend on the waiting time $T_i$. In the case where $R_i$ and $T_i$ are independent, the continuous-time random walk is said to have decoupled memory [52]. To specify the model, one has to make a choice for the joint probability density $\phi(r,t)$ for the pair $(R_i, T_i)$. The marginal densities are given by

$$f(r) = \int_0^\infty \phi(r,t)\mathrm{d}t, \quad g(t) = \int_{-\infty}^\infty \phi(r,t)\mathrm{d}r.$$

The discrete time and space case as presented in Section 3.1 can be obtained as a special case by choosing $f$ and $g$ to contain Dirac delta components. The position of the random walker is given by the sum of the individual jumps

$$\tilde{R}_t = \sum_{i=0}^{N_t} R_i,$$

where $N_t$ is the total number of jumps up to time $t$, given by $N_t = \max\{k : \sum_{i=0}^k T_i \leq t\}$. It is of interest to find the probability density $p(x,t)$ of $\tilde{R}_t$. By writing $\Phi(t) = 1 - \int_0^t g(s)\mathrm{d}s$, namely the probability that the random walker pauses at least time $t$ before leaving the site, one can derive a master equation for $p$ as follows [89, 63]:

$$p(x,t) = p(x,0)\Phi(t) + \int_0^\infty g(t-t')\left(\int_{-\infty}^\infty f(r)p(x-r,t')\mathrm{d}r\right)\mathrm{d}t'. \tag{3.4}$$

The terms on the right hand side describe all the possible ways in which a walker can be at position $x$ at time $t$. The first term describes a walker that started at $x$ at time $t = 0$ and did not move, and the integral accounts for all possible ways a particle can move into $x$ given a jump of size $r$ occurred at time $t'$. In addition to the assumption of the walk being decoupled, it has been shown that assuming that the waiting times are exponentially distributed (making the times for jumps a Poisson process), as well as Gaussian jumps with 0 mean and variance $\sigma^2$, leads to approximate solutions to (3.4) of the form

$$p(x,t) = \frac{1}{\sqrt{4\pi\lambda\sigma^2 t}} e^{\left(-\frac{x^2}{4\lambda\sigma^2 t}\right)}, \tag{3.5}$$

namely solutions to the diffusion equation (3.3) with $D = \lambda\sigma^2$. The solution method [62] is based on taking the Laplace and Fourier transform of Equation (3.4), and in doing so it has been shown that (3.5) holds for any probability density functions with finite characteristic waiting time and jump length variance,

i.e.

$$\int_0^\infty g(t)t\mathrm{d}t < \infty,$$
$$\int_{-\infty}^\infty f(r)r^2\mathrm{d}r < \infty.$$

The decoupled CTRW has been extended for more general probability density functions $f$ and $g$, as well as various dependencies between the two. An example is to model time-dependent jump lengths [89, 83], which can be used in biological applications, where the movement of an individual becomes larger the longer it rests between movement. Various other assumptions can lead to fractional orders of both spatial and temporal derivatives, referred to as fractional diffusion [54].

### 3.1.2 The correlated random walk

The previous types of random walks discussed, both on a lattice or governed by a more general jump distribution, are such that the position of the walker is subject to random jumps. There is an alternative type of random walk, called the velocity-jump process or a correlated (or persistent) random walk [35, 71, 17], where it is the velocity of a walker that is subject to random changes. A walker is characterized not only by its position $x$ at time $t$, but also its velocity $v$. The process is described by two probability density functions, one for the times of velocity changes, and one for the randomly chosen velocities. This type of random motion found applications in biology in the 1970's, as a model of the run-and-tumble motion of *E. coli* and chemotaxis [6, 4].

The most simple correlated random walk was described by Goldstein in 1951 [35] and is concerned with a population of non-interacting walkers in one spatial dimension. The mathematical setup is as follows [17]: Consider separately a population of left- and right-moving walkers at position $x$ at time $t$. Denote by $L(x,t)$ and $R(x,t)$ the density of non-interacting walkers (or the probability density of a single walker) in the left and right directions respectively. The speed is assumed to be constant, and each walker reverts direction at times governed by a Poisson process with intensity $\lambda$. To derive partial differential equations for the densities $L$ and $R$, we may discretize time into small time-steps of duration $\Delta t$. For $\Delta t$ small enough, such that the probability of a walker making two or more turning events in a time interval of length $\Delta t$ is negligible, the probability of a turning event is approximated by $\lambda\Delta t$. After a walker has had an opportunity to turn, it moves a distance $\Delta x$ in its current direction. The expressions of the densities forward in time are then given by

$$L(x,t+\Delta t) = \lambda\Delta t R(x+\Delta x,t) + (1-\lambda\Delta t)L(x+\Delta x,t),$$
$$R(x,t+\Delta t) = \lambda\Delta t L(x-\Delta x,t) + (1-\lambda\Delta t)R(x-\Delta x,t).$$

The two equations are analogous to the master equation (3.1) for the simple random walk described in Section 3.1. Expanding these as Taylor series and

taking the limit $\Delta x, \Delta t \to 0$ such that $\Delta x/\Delta t \to s$ we obtain the system

$$\frac{\partial L}{\partial t} = s\frac{\partial L}{\partial x} - \lambda(L - R),$$
$$\frac{\partial R}{\partial t} = -s\frac{\partial R}{\partial x} + \lambda(L - R).$$

At this point we have obtained two separate equations for the left- and right-moving walkers respectively. A relevant question is whether we can find an equation for the density of walkers, regardless of direction. In fact we can do so, by manipulating the equations. We derive two new equations by first adding the two equations and then differentiating with respect to $t$, and next we subtract the equation for $R$ from that of $L$ and differentiate with respect to $x$, and obtain

$$\frac{\partial^2(L + R)}{\partial t^2} = -s\frac{\partial^2(L - R)}{\partial t \partial x},$$
$$\frac{\partial^2(L - R)}{\partial t \partial x} = s\frac{\partial^2(L + R)}{\partial x^2} - 2\lambda\left(\frac{\partial(L - R)}{\partial x}\right).$$

By substituting the second equation into the first and using the original equations, we finally obtain the following equation for the total density $p(x, t) = L(x, t) + R(x, t)$

$$\frac{\partial^2 p}{\partial t^2} + 2\lambda\frac{\partial p}{\partial t} = s^2\frac{\partial^2 p}{\partial x^2}, \tag{3.6}$$

which is known as the telegraph equation. One can see that it looks similar to the diffusion equation, except it contains an additional second order time derivative of $p$. However, there is a limiting procedure known as the parabolic limit [67], which will result in the diffusion equation. By dividing Equation (3.6) by $2\lambda$ one obtains

$$\frac{1}{2\lambda}\frac{\partial^2 p}{\partial t^2} + \frac{\partial p}{\partial t} = \frac{s^2}{2\lambda}\frac{\partial^2 p}{\partial x^2}.$$

Recall that $\lambda$ is the rate parameter of the Poisson process governing turning event, and the mean time between turning is therefore $1/\lambda$. By taking the limits $\lambda \to \infty$ and $s \to \infty$ in such a way that $s^2/2\lambda = D$ is constant, the telegraph equation reduces to the diffusion equation. This can be intuitively interpreted as the limit of turning events occurring more and more frequently at the same time as the speed increases.

This type of scaling is sometimes referred to as a "large-time diffusion approximation". The reason is that the limit becomes a good approximation for long times where the random walkers have performed a large number of turning events.

To demonstrate the connection between the simple random walk and the correlated random walk we perform simulations, with parameters chosen to result in the same diffusion coefficient $D$, in both the case of the simple random walk from Section 3.1 as well as the correlated random walk described here. We compare the stochastic simulations to the solution of the corresponding

diffusion equation. The simulation show that the stochastic simulation agree well with the solution to the PDE for both the random walk on a lattice (Figure 3.1) and for the correlated random walk on a lattice (Figure 3.2). The initial position of the random walkers are given by a Gaussian distribution, and in the case of the correlated random walk, each walker's initial velocity is chosen randomly with equal probability.

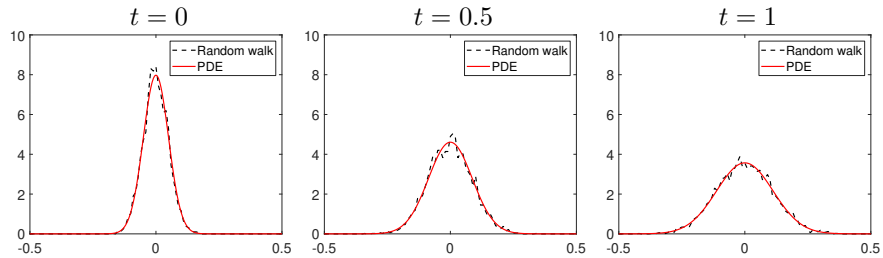


**Figure 3.1:** Comparison between stochastic simulation of the random walk on a lattice with $\Delta x = 0.01$, $\Delta t = 0.01$, simulated with $5000$ walkers for $1$ unit of time. Parameter choices result in $D = 0.01$.

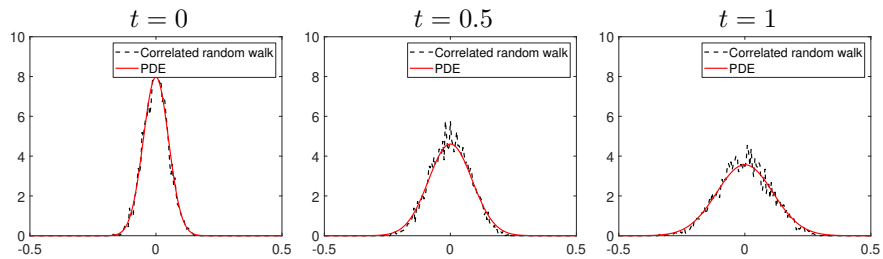


**Figure 3.2:** Comparison between stochastic simulation of the correlated random walk on a lattice with $\Delta x = 0.005$, $\lambda = 10$ and $D = 0.01$ making $\Delta t = 0.0158$, simulated with $5000$ walkers for $1$ unit of time.

To illustrate the importance of a large $\lambda$ in the correlated random walk, we can investigate how a smaller $\lambda$ influence the behaviour. We also vary $\Delta t$ in such a way that the fraction $s^2/\lambda = D$ is the same for all choices of $\lambda$. It can be seen in Figure 3.3 that when using a smaller $\lambda$, the process does not appear to be entirely driven by diffusion. In the third image of Figure 3.3 one can distinguish two peaks on the left and right sides of the origin. These are the results of the left-moving and right-moving walkers not having turned in the short time up to that point. This highlights the importance of the assumption that $\lambda \to \infty$, or equivalently, that the walkers have performed a large number of turning events in the timeframe of observation, when using the diffusion approximation.

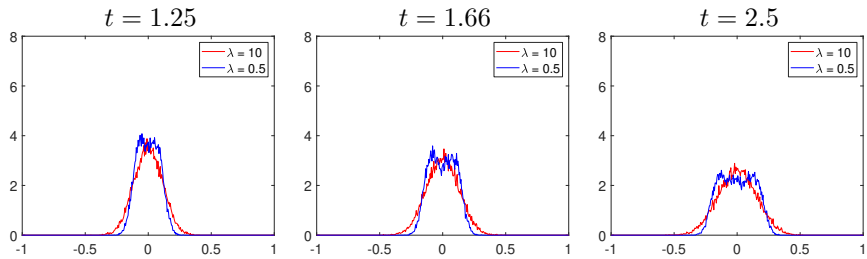


**Figure 3.3:** Stochastic simulation of the correlated random walk with different turning intensities $\lambda$.

## 3.2 More complicated random walks - External bias and individual interactions

Completely random motion is seldom a realistic description of biological motion. Two reasons are that individuals interact with each other, and that they interact with their environment in which they move. The previous models can be used to model a large population of non-interacting cells, but if there is reason to believe that the interactions between cells are of importance, one must develop the models and incorporate those effects as well.

One of the most simple types of interaction between cells is volume exclusion, i.e. that cells take up space and potentially obstruct the motion of other cells. This can be modelled in the random walk framework by introducing a carrying capacity that limits the number of cells allowed in each lattice site. The most restrictive case is where only a single cell is allowed to occupy each site. In order to demonstrate some of the difficulties that arise when accounting for this, we use the unbiased simple random walk on the lattice described in Section 3.1, but assume that a walker does not move into a space that is occupied. We denote by $P(x,t)$ the density of a walkers at position $x$ at time $t$, of a large number of walkers without any interactions apart from volume exclusion.

In order to write down the expression for $P$ at time $t + \Delta t$ we need to consider the ways in which a walker can end up at $x$ at time $t + \Delta t$. That can happen if a walker residing at $x \pm \Delta x$ makes a jump of $\mp\Delta x$, and if the lattice at $x$ is empty. Without any further assumption, one needs to introduce a 2-point distribution function that contains the information about the occupancy of pairs of lattice sites [84]. This allows us to express the probabilities of a site being occupied *and* its neighbouring site being vacant. The explicit modelling of spatial correlations typically result in an increasing number of equations. The reason is that in order to find a 2-point distribution function, one needs the 3-point distribution function and so on. Techniques referred to as moment closure approximations can be used to truncate such system of equations [84]. The most common approach to work around the issue of spatial correlations is to assume independence of the vacancy of pairs of lattice sites. Mathematically one assumes that the event of site $x \pm \Delta x$ being occupied and site $x$ being vacant

are independent and therefore that the probability is given by the product of the two events. This is a common method known as the mean-field approximation. For our simple unbiased random walk this results in

$$P(x,t+\Delta t) = \frac{1}{2}P(x-\Delta x,t)(1-P(x,t)) + \frac{1}{2}P(x+\Delta x,t)(1-P(x,t)),$$

and following the same limiting procedure as in Section 3.1 we obtain the equation

$$\frac{\partial P}{\partial t} = D(1-P)\frac{\partial^2 P}{\partial x^2},$$

for a density $P$ such that $(1-P) \geq 0$. We can see that the rate of diffusion is dependent on the cell density.

The correlated random walk has also been extended to include volume exclusion [90], as well as proliferating random walkers [91].

Apart from the interaction between walkers, one can also model various types of external biases. Phenomena such as chemotaxis or durotaxis can be modelled using a biased random walk, where it is assumed that the bias $q$ in Equation 3.1 is a function $q(C(x))$ of the external field $C(x)$ (such as chemical concentration or substrate stiffness). The choice of how the bias depends on the external field is one of the important modelling questions.

A good example where it is important to incorporate information about the cells' local environment is when one is modelling brain tumors such as glioblastoma. The models typically take the form of reaction-diffusion equations which describe the time evolution of the density of cells in the tissue. As a step towards a more realistic model, one can use a spatially varying diffusion coefficient; one in white matter and one in grey matter. This has been done and was motivated by the fact that the tumor spread velocity differed significantly between regions made up of grey or white matter [87]. The concept of heterogeneous diffusion can be generalized further by modelling the tumor spread as anisotropic diffusion, described below. This has been done in the context of brain tumors [45, 70], where diffusion tensor imaging (DTI) of the brain is used to derive the model of cell migration. DTI is a magnetic resonance imaging technique which measures the restricted diffusion of water in tissues such as the brain, resulting in a diffusion tensor that varies between voxels. A diffusion tensor is a $3 \times 3$ array of numbers (matrix), represented by

$$\mathbf{D} = \begin{pmatrix} D_{xx} & D_{xy} & D_{xz} \\ D_{yx} & D_{yy} & D_{yz} \\ D_{zx} & D_{zy} & D_{zz} \end{pmatrix},$$

which is symmetric, meaning that $D_{xy} = D_{yz}$, $D_{xz} = D_{zx}$ and $D_{yz} = D_{zy}$, and is therefore described by 6 unique elements. The diffusion is isotropic in the case where all three diagonal entries are equal, $D_{xx} = D_{yy} = D_{zz}$, and all off-diagonal entries are 0, and anisotropic otherwise.

From the tensor, a number of measures can be derived which give insights into the anatomy of the brain. A central challenge in using DTI data in a model

of cell migration is to determine how the diffusivity of water translates into migratory cues for cells. If the motility of cells behaved exactly like diffusing water, the diffusion tensor could be used without modifications, but this is clearly not the case. Some work has been done on the topic, in particular in the context of modelling the density of cells using partial differential equations [70, 86, 2, 45], but less has been done when using agent-based models. In **Paper III** we develop an agent-based model of migrating cancer cells in the brain of mice, where the migration is guided by DTI data. We investigate how the parameters governing proliferation, migration and anisotropy influence the tumor spread velocity. We also compare model simulations to microscopy images of brain tumors in mice.

## 3.3 A more detailed cell model

Although the previously described random walk models can be extended in a large number of ways to model interactions between multiple cells and between the cells and their local environment, a weakness lies in the fact that the cells are effectively modelled as points in space, or as entities occupying discrete lattice sites. In this section we describe our model of a cell used in **Papers I** and **II**, and show that it offers an alternative way to model cell motion, which enables more complicated and realistic interactions between cells and their environment. We also explore its relationship to the previously described random walks. First we present the most simple version of the model, and we then discuss how it can be generalized as was done in **Papers I** and **II**.

We model a cell moving along a one-dimensional fiber as having two adhesion sites located at positions $x_1$ and $x_2 \in \mathbb{R}$, which both connect to the cell nucleus denoted by $\mu \in \mathbb{R}$. As cells are able to exert forces on the ECM, we assume that each adhesion site is connected to the nucleus with an elastic spring of rest length 0. For now we assume that both spring coefficients are equal, and denoted by $\alpha$. The force exerted by the cell at adhesion site $i$ is given by

$$F_i = \alpha(\mu - x_i). \tag{3.7}$$

A cartoon illustration of a cell can be found in Figure (3.4).

In equilibrium the position of the cell nucleus is given by

$$\mu = \frac{x_1 + x_2}{2}, \tag{3.8}$$

which is the center of mass of the two adhesion sites. The cell migrates by updating the position of its adhesion sites at times governed by a Poisson process with rate $\lambda$, each site independent of the other. Once an update occurs, its new position is chosen form a normal distribution centered around the current nucleus position, with variance $\sigma^2$. It is assumed that adhesion site jumps are instantaneous, and that the new nucleus position, given by Equation (3.8), is attained without delay.

This mathematical model of a migrating cell can be considered a special case

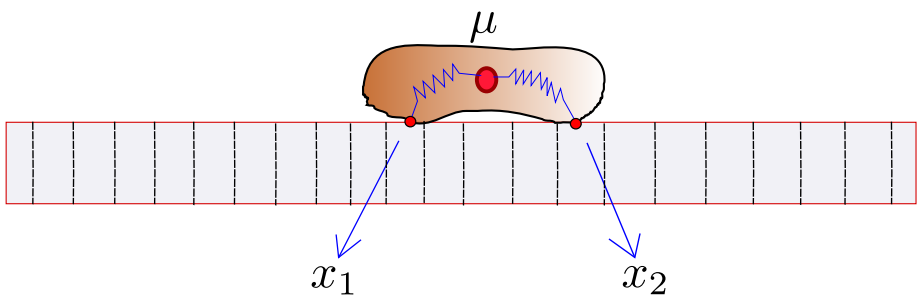


**Figure 3.4:** Cartoon illustration of a migrating cell in one spatial dimension.

of a model introduced by Dallon [21] in 2013. In the original model cells migrate in 2D and have a variable number of adhesion sites which can be attached or detached to the substrate, and the position of the cell nucleus is given by an ordinary differential equation derived from Newton's second law of motion. A so-called "centroid-model" derived from the full model was presented in a separate paper [20], in which it was assumed that the equilibrium position of the nucleus is attained instantaneously. A detailed discussion of how our model relates to the original model by Dallon is provided in **Papers I** and **II**.

Our cell model can be simulated using a stochastic simulation algorithm similarly to the simulation of a random walk. At each time step when a position change will take place, instead of simply computing its new position (and velocity in the case of a correlated random walk), we first need to choose the adhesion site which will be updated, compute its new position and finally compute the new position of the cell nucleus. As the cell nucleus changes position only as a consequence of an adhesion site changing its position, we may ask whether this model of cell migration can be analysed in a fashion similar to the classical random walk models, with the goal of arriving at a macroscopic description in the form of a partial differential equation. We will now show that this is indeed the case.

In order to proceed we first make the following observation. Because each of the two adhesion sites update their positions independently of each other, according to a Poisson process with rate parameter $\lambda$, one can equivalently consider $\Lambda = 2\lambda$ the rate parameter of the Poisson process governing the time of "any event", and that when such an event occurs, one of the two sites is chosen uniformly at random. By considering the nucleus position to be the position of the cell, $x$, we write an expression for the probability density $p(x, t + \Delta t)$ of a migrating cell at position $x$ at time $t + \Delta t$, analogous to Equations (3.1) and (3.2):

$$p(x, t + \Delta t) = e^{-\Lambda\Delta t} p(x, t) + (\Lambda\Delta t) e^{-\Lambda\Delta t} \int_{\mathbb{R}} p(x - r, t) f(r) \mathrm{d}r + \mathcal{O}(\Delta t^2), \quad (3.9)$$

where $f(r)$ is the probability density of a cell nucleus jump of length $r$. The first term on the right hand side correspond a cell already being located at $x$

at time $t$, and performing no jumps in the time interval $[t, t+\Delta t]$. The second term correspond to a cell making exactly one jump in the time interval, and all possible ways to jump from $x-r$ into $x$. The remainder correspond to events where two or more jumps occur in the time interval, which will become negligible as $\Delta t \to 0$. In order to make headway we need to determine $f$. Recall that we have assumed that the new position of a single adhesion site is normally distributed around the current nucleus position, whereas $f$ describes how the new nucleus position is distributed.

We consider how the nucleus moves as one of the two adhesion sites moves. Let $x_1$ and $x_2$ be the current adhesion site positions, and $\mu$ the current nucleus position. Assuming that the first site updates its position into $x_1^+ = \mu + W$, where $W$ is a normal random variable with mean 0 and variance $\sigma^2$ we have the change in nucleus position given by:

$$\begin{aligned}\mu^+ - \mu &= \frac{x_1^+ + x_2}{2} - \frac{x_1 + x_2}{2} \\ &= \frac{\mu + W + x_2}{2} - \frac{x_1 + x_2}{2} \\ &= \frac{\frac{x_1+x_2}{2} + W}{2} - \frac{x_1 + x_2}{2} \\ &= \frac{x_2 - x_1}{4} + \frac{W}{2}.\end{aligned}$$

Similarly, in the case that site 2 makes a jump, we obtain

$$\mu^+ - \mu = \frac{x_1 - x_2}{4} + \frac{W}{2}.$$

This shows that the size of the nucleus jump, as a consequence of the change of one of its adhesion sites, depends on the distance between the current sites. This is due to the fact that new sites are chosen around the nucleus position, and not around its own current position. For an intuitive understanding, consider a cell that happens to be much larger than its typical size, then the distance between one of its current sites and the nucleus is large, resulting (on average) in a jump size which is large.

By introducing the quantity $y = (x_2 - x_1)/2$, we observe that when site 1 makes a jump, the change in nucleus position is normally distributed with mean $y/2$ and variance $\sigma^2/4$, and when site 2 makes a jump the change in nucleus position is normally distributed with mean $-y/2$ and variance $\sigma^2/4$. Therefore, the probability density for a nucleus jump, conditioned on the current distance $y$ is given as a mixture-distribution with weights $1/2$ as each jump is equally likely:

$$f(r \,|\, y) = \frac{1}{2}\frac{1}{\sqrt{\pi\sigma^2/4}} e^{-\frac{(r-y/2)^2}{\sigma^2/4}} + \frac{1}{2}\frac{1}{\sqrt{\pi\sigma^2/4}} e^{-\frac{(r+y/2)^2}{\sigma^2/4}}.$$

In order to find an expression for the unconditional density function $f(r)$ governing the size of nucleus jumps, we need also consider how the distance $y$ is distributed. In the appendix of **Paper I** we show that when the initial distance

$(x_2 - x_1)/2$ is normally distributed, the distribution after many steps converges to a normal distribution with mean 0 and variance $\sigma^2/3$, and we can therefore find $f(r)$. We use $g(y)$ to denote the probability density function of the distance between adhesion sites. For now, taking this fact for granted, we can investigate $f(r)$ by writing

$$\begin{aligned} f(r) &= \int_{-\infty}^{\infty} f(r \,|\, y) g(y) \mathrm{d}y \\ &= \int_{-\infty}^{\infty} \left( \frac{1}{2} \frac{1}{2\sigma\sqrt{2\pi}} e^{-\frac{(r-y/2)^2}{\sigma^2/4}} + \frac{1}{2} \frac{1}{2\sigma\sqrt{2\pi}} e^{-\frac{(r+y/2)^2}{\sigma^2/4}} \right) \frac{1}{\sqrt{2\pi\sigma^2/3}} e^{-\frac{y^2}{2\sigma^2/3}} \mathrm{d}y \\ &= \frac{1}{\sqrt{2\pi\sigma^2/3}} e^{-\frac{r^2}{2\sigma^2/3}}, \end{aligned}$$

which is the probability density function of a normal distribution with 0 mean and variance $\sigma^2/3$. We have obtained $f(r)$ and can proceed to use it in Equation (3.9). Note that in finding $f$ we have assumed that the distribution of distances $y$ has converged. A formula for how the distribution changes after each step can be found in the Appendix of **Paper I**.

We are now in a position to work with Equation (3.9), in order to investigate the long time behaviour of the model. Since the detailed derivation is presented in **Paper I**, to avoid repetition we do not include it here. However, it is worth mentioning that the derivation relies on scaling arguments analogous to those of a random walk on a lattice, namely small jumps of high frequency. This results in a diffusion equation for probability density $p(x,t)$ of a migrating cell at position $x$ at time $t$ given by

$$\frac{\partial p}{\partial t} = \lambda \frac{\sigma^2}{3} \frac{\partial^2 p}{\partial x^2}. \tag{3.10}$$

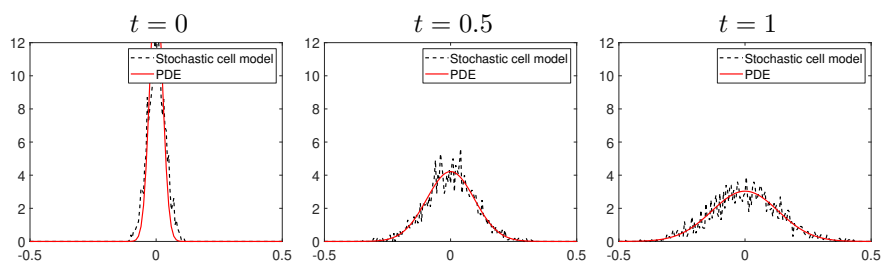


**Figure 3.5:** Comparison between stochastic simulation of our cell model for $\lambda = 20$, $\sigma = 0.05$, $\Delta t = 0.01$ resulting in $D = 0.0083$, simulated with 2000 walkers for 1 unit of time.

A comparison between stochastic simulations and solutions to the corresponding diffusion equation (3.10) is provided in Figure 3.5, showing good agreement. It confirms that the assumption that the distance between adhesion

sites has converged is reasonable (for the chosen parameters) in deriving the PDE.

In our example we saw that the probability of the nucleus to perform a jump of a particular size $r$ depends on the distance between the sites, and this is an inherent feature of the model since new adhesion sites are chosen to be randomly distributed around the nucleus position. However, if one were to model more complicated interactions between cells and the environment, $f$ becomes a function of either the nucleus position, or a function of the exact position of the two adhesion sites. In this case it is not clear when it is possible to derive a macroscopic description in the form of a PDE.

The most basic model presented here can be extended in a number of ways. In particular it can be used to model durotaxis, which we have done in **Papers I** and **II**. We use the model to investigate two different possible mechanisms contributing to the durotactic response of cells. In **Paper I** we investigate the hypothesis that cells sense the stiffness of the substrate, and that the adhesion sites become reinforced and remain longer on stiff substrates, as has been discussed in the literature [73] and demonstrated in experiments [31]. We do that by introducing a function $E(x)$ describing the stiffness of the substrate. We then extend the model to allow for spatially varying adhesion jump rates $\lambda = \lambda(E(x))$ in such a way that adhesion sites remain for longer periods of time on stiff substrates. We investigate two different mechanisms for cell sensing, and conduct an analysis of the model, deriving a drift-diffusion equation for the density of cells. We find that the drift velocity toward stiffer regions depends on the ratio between the stiffness $E$ and its gradient $E'$. Furthermore, we demonstrate that the model is able to reproduce results from experiments, where cells are migrating on a substrate with a periodically varying stiffness profile. In this case the cells cluster on the regions of high stiffness. In **Paper II** we also extend the basic model presented in this section to model a cell migrating on an elastic substrate that deform as the cell exerts forces. Moreover, we allow the cell spring coefficients to be functions of the stiffness $\alpha = \alpha(E(x_i))$. We investigate different relationships which have been observed in the literature, where cells can generate larger forces on stiffer substrates. In this case the cells migrate up the stiffness gradient.

Although the phenomena of migrating cells moving preferentially towards stiffer regions is likely the result of multiple mechanisms, our modelling demonstrates that both reinforcement of adhesion sites and stiffness-dependent forces can cause a net movement up a stiffness gradient. The modelling of **Paper I** also encourages a new type of experiment which, to the best of my knowledge, has not yet been conducted but can be performed. In the study by Fusco et al. [31] the average lifetime of adhesions was measured, for cells seeded on substrates of three different but uniform rigidities. However, the same study could be performed on substrates with a gradient, providing insights into whether or not a significant difference in lifetimes exists along the length of the cell. Our model provides estimates of how large the difference in average lifetime needs to be in order to result in a significant durotactic drift.

## 3.4 Using a microscopic or macroscopic model

So far we have only looked into one group of models, based on random walks, but there exists a large number of other modelling approaches in the literature. Many of these models are discussed in the appended papers. Here we briefly discuss strengths and weaknesses of different models, and mention other common models of cell migration.

There is no universal way to categorize all the different models of cell migration, but a good way to think about them is in terms of the level of detail they contain, or the temporal and spatial scale of interest. The simple random walk models can be regarded as an intermediate scale, where the entities of interest are individual cells and the relevant processes are those governing the rules of motion. We demonstrated how one can derive a corresponding macroscopic level description in the form of one or several partial differential equations governing the time evolution of a population of cells. Because the macroscopic models are deterministic they are typically most useful in studying large populations of cells where the stochastic effects of individual cells are not of great importance. The macroscopic models are often in the form of diffusion equations with population growth [85, 87]. They can also take the form of mixture-models, in which a number of mixtures, or phases, are considered. These typically include healthy cells, tumor cells, extracellular matrix and blood vessels [9, 42]. Equations are derived from mass balance equations along with constitutive laws to model various biophysical properties.

The cell model we presented in the previous section takes one step towards a more detailed model, including intracellular details of the dynamics of adhesion sites and forces generated by the cell. Interestingly enough we saw that the population level description agreed with those obtained from the standard random walk or the correlated random walk in the absence of environmental cues.

These derivations are special in the sense that they provide a link between the parameters at the individual level to those at the population level. This is a highly desirable feature for a number of reasons. Firstly, it is often the case that experimental measurements are obtained on the cellular level (migration velocities, turning rates, etc.), and parameters at the level of the cell are often more easily interpreted and matched to such experiments. Secondly, the connection between the individuals and the population offers useful insights into understanding the underlying mechanisms. It is often the case that many different individual level mechanisms can produce the same population level behaviour. As a result, fitting a population level model to data, such as a reaction diffusion equation, may not offer as much insight into the underlying phenomena governing the system. However, such models of course have their use, in particular when it comes to making predictions. They can also be useful in estimating population level quantities of for example the spread and growth of tumors. It should also be noted that the task of deriving a population level model from an individual based one is no trivial task, and may very well be impossible in some cases.

Another commonly used model of cell migration is the cellular Potts model

(CPM) [59]. It is a grid-based model where a cell is defined to occupy multiple lattice sites, with constraints acting on the total cell area (i.e. the total number of sites it occupies). Each cell is associated with a unique index, used to keep track of the lattice points belonging to a certain cell. The temporal dynamics of the model is governed by a Hamiltonian function describing the energy of a configuration. When an update event takes place, a random site is chosen and is given the opportunity to change into the state of one of its neighbours. If the new configuration results in a decrease in energy, it is accepted. Configurations with a higher energy are accepted with a probability determined by the change in energy.

A strength of cellular Potts models lies in its versatility. It can be extended to model more complicated phenomena related to cell-cell adhesion, which is done by modifying the Hamiltonian. It is also possible to couple it with mechanical models of the extracellular matrix [88], or chemotaxis [82].

Yet another group of models are the computational models including a great amount of biophysical details [57, 97, 25]. In [51] a 3D ECM is modelled explicitly as a network of viscoelastic fibers, which deforms as a cell exerts forces and migrates through it. The intracellular dynamics are governed by equations for the focal adhesion dynamics, several equations for the cell membrane as well as the contractile motion of actin stress fibers. Other models focus more on the dynamics of adhesion sites, in combination with deformable substrates [96]. The strength of using models with a lot of detail is that they are able to be much more realistic. However, the drawback is that they are difficult or even impossible to analyse mathematically, and can be computationally demanding.

## 3.5 Models of cell polarization

In Section 2.2 we described the phenomena of spontaneous symmetry breaking, and mentioned that it is often modelled using a reaction-diffusion system of the interacting species (active and inactive Cdc42). In many models, the GDP- and GDI-bound forms of Cdc42 are not discerned, and Cdc42 is considered to be active or inactive (see Figure 2.1). Moreover, the spatial dimension is often assumed to be one-dimensional, motivated by the fact that polarization occurs along a single axis of "front-back" orientation. Therefore, the spatial distribution of Cdc42 can be considered either along the diameter of a cell, or along the circumference.

An example of such a system can be found in [68, 64], which is a mass-conserved reaction-diffusion system of two species u and v:

$$\begin{aligned} \frac{\partial u}{\partial t} &= D_u \frac{\partial^2 u}{\partial x^2} - f(u,v), \\ \frac{\partial v}{\partial t} &= D_v \frac{\partial^2 v}{\partial x^2} + f(u,v), \end{aligned} \tag{3.11}$$

where $u = u(x,t)$ and $v = v(x,t)$ denote the concentration at position $x$ at time $t$ of species u and v respectively. The reaction term $f$ is assumed to depend on the concentrations $u$ and $v$. The domain in one spatial dimension often takes the

form of a closed interval $I = [0, L]$ along with zero-flux boundary conditions [64]

$$\left.\frac{\partial u}{\partial x}\right|_{x=0,L} = \left.\frac{\partial v}{\partial x}\right|_{x=0,L} = 0,$$

in the case of modelling the diameter of a cell. One may use periodic boundary conditions in the case the domain represents the circumference of a cell. In either case the total amount of Cdc42 in the system is conserved.

The reaction function $f$ encompasses the conversion between $u$ and $v$. The particular choice of such a function result in different dynamics of the system, and multiple choices have been used and motivated in the literature. The precise form of the interactions remain unclear, and in [36] six classes of models were discussed.

It has been proposed that a Turing-type mechanism might be responsible for spontaneous symmetry breaking, and the resulting local accumulation of active Cdc42 at a particular site at the membrane. A reaction-diffusion system is said to exhibit a Turing-instability, or diffusion-driven instability, if a homogeneous steady state $(u_0, v_0)$ (in the absence of diffusion) is stable to small perturbations, but unstable to small spatial perturbation in the presence of diffusion [65].

Consider the following system, which is a non-dimensional version of an arbitrary 2-species reaction-diffusion system:

$$\begin{aligned}\frac{\partial u}{\partial t} &= \frac{\partial^2 u}{\partial x^2} + \gamma f(u, v),\\ \frac{\partial v}{\partial t} &= d\frac{\partial^2 v}{\partial x^2} + \gamma g(u, v),\end{aligned}$$

where $d$ is the ratio of diffusion coefficients $d = D_v/D_u$, and $\gamma$ can be interpreted as the relative strength of reaction terms.

The conditions for diffusion-driven instability [65] are formulated in terms of the partial derivatives of $f$ and $g$ evaluated at the relevant steady state $(u_0, v_0)$

$$f(u_0, v_0) = 0,\ g(u_0, v_0) = 0,$$

and are given by

$$\begin{aligned}&(i)\ f_u + g_v < 0, && (ii)\ f_u g_v - f_v g_u > 0,\\ &(iii)\ df_u + g_v > 0, && (iv)\ d(f_u + g_v)^2 - 4d(f_u g_v - f_v g_u) > 0,\end{aligned}$$

where all partial derivatives are evaluated at the steady state. These four conditions are derived from a linear stability analysis, requiring that the steady state is stable in absence of diffusion (criteria $(i)$ and $(ii)$), and unstable in the presence of diffusion (criteria $(iii)$ and $(iv)$).

Two remarks are in order. The first is that the diffusion coefficient $d$ cannot be equal to 1, since in that case both criteria $(i)$ and $(iii)$ together form a contradiction. This implies that systems where both species diffuse at the same rate cannot satisfy the above criteria. The second remark is that systems of the form 3.11, where $g = -f$, never satisfy criteria $(ii)$. Nevertheless, there are models

with mass conservation that exhibit pattern formation, for example through a mechanism known as wave-pinning [64], where a moving concentration front decelerates and becomes stationary or pinned.

More recently, a new group of models referred to as bulk-surface models [75, 76, 19] have emerged, in which the cell is modelled as a spherical volume in 3D. The cell is modelled as having a bulk (cytosol) $\Omega$ and a surface (cell membrane) $\Gamma$, where the GDI-bound Cdc42 is assumed to exist in the bulk, and the GDP- and GTP-bound forms exist on the membrane. The three concentrations of interest are therefore described by the three functions

$$\begin{aligned} V &: \Omega \times [0,T] \to \mathbb{R} && \text{Concentration of GDI-bound Cdc42} \\ v &: \Gamma \times [0,T] \to \mathbb{R} && \text{Concentration of GDP-bound Cdc42} \\ u &: \Gamma \times [0,T] \to \mathbb{R} && \text{Concentration of GTP-bound Cdc42} \end{aligned}$$

and the reaction-diffusion system governing the concentrations takes the general form [74]:

$$\begin{aligned} \frac{\partial V}{\partial t} &= D_V \Delta V, \quad \mathbf{x} \in \Omega, t > 0 \\ \frac{\partial u}{\partial t} &= D_u \Delta_\Gamma u + \gamma f(u,v), \quad \mathbf{x} \in \Gamma, t > 0 \\ \frac{\partial v}{\partial t} &= D_v \Delta_\Gamma v + \gamma(-f(u,v) + q(u,v,V)), \quad \mathbf{x} \in \Gamma, t > 0 \end{aligned} \tag{3.12}$$

along with the association and dissociation of inactive Cdc42 at the membrane, described by the flux boundary condition for $V$ at the boundary $\Gamma$:

$$-D_V[(\nabla V)^T \cdot \mathbf{n}] = q(u,v,V). \tag{3.13}$$

This formulation of the cell as a 3D object with a cytosol and a membrane is more realistic than the one-dimensional models. Criteria for pattern formation analogous to those presented above have been derived for bulk-surface models [76, 74]. One of the most interesting feature of these conditions is that it is possible to satisfy the criteria for Turing-instability even when the diffusion rates are equal, $D_u = D_v$.

### 3.5.1 Comparison between models

We now go on to describing the particular choices for $f$ and $q$ used in the paper by Rätz and Röger [75] and discuss how our choice of reaction function $f$ used in **Paper IV** is different from theirs.

Recall that apart form the three concentrations of interest, $V, v$ and $u$, two key players are GEFs, promoting activation, and GAPs, promoting inactivation. The choice of reactions chosen in [75] are best understood by starting from the schematic representation shown in Figure (3.6).

We start with the function $q$, implemented as a flux boundary condition in (3.13), governing the conversion between cytosolic GDI-bound form denoted

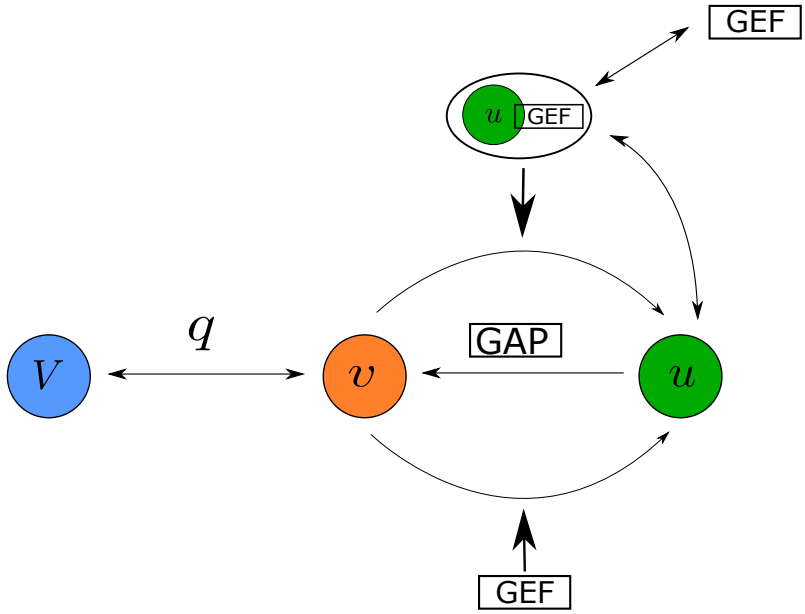


**Figure 3.6:** Schematic illustration of the interactions between $V$, $v$ and $u$ of the model in [75]. The image is re-drawn based on the schematic representation in [75].

by $V$, and the GDP-bound form, $v$, at the membrane. It is defined by

$$q(V, v, u) = b_1 \frac{|\Omega|}{|\Gamma|} V \cdot (c_{max} - u - v)_+ - b_{-1} v, \tag{3.14}$$

where $b_1$ and $b_{-1}$ are the adsorption/desorption coefficients. The first term is treated as a reaction between $V$ and a free site on the membrane, where $c_{max}$ denotes a saturation value, above which no adsorption occurs. The notation $(\cdot)_+$ denotes the positive part of the expression inside the parentheses. Conversion from the GDP-bound form $v$ into the cytosol, $V$, is taken to be proportional to the concentration $v$, resulting in the second term. In our model we use the same $q$, with the difference that we do not exclusively use the positive part of $(c_{max} - u - v)$.

Let us now proceed to the particular choice of $f$ used in [75]. In what follows we begin by only considering the reaction parts of the full system (3.12), and will lastly add diffusion to the equations.

It is assumed that activation can be catalyzed by both GEF and by an effector-GEF-GTPase complex consisting of one GEF molecule and one molecule of active Cdc42, $u$. Therefore, two additional concentrations are introduced:

| | |
|---|---|
| $m : \Gamma \times [0, T] \to \mathbb{R}$ | Concentration of membrane-bound effector-GEF-GTPase complex |
| $g : \Gamma \times [0, T] \to \mathbb{R}$ | Concentration of membrane-bound GEF |

In both cases of activation, it is assumed that the rates of activation are proportional to $v$ and the catalyst. The concentration of GAPs are not taken into account, and a Michaelis-Menten law is assumed for the kinetics of inactivation. These assumptions result in the rate of change of $v$ given by

$$\left[\frac{\partial v}{\partial t}\right]_{\text{reaction}} = -k_1 vg - k_2 vm + k_3 \frac{u}{u + k_4},$$

where the first term corresponds to the activation due to GEF alone, the second term due to the effector-GEF-GTPase complex, and the third term the inactivation rate resulting from the assumption of Michaelis-Menten kinetics. $k_1$, $k_2$, $k_3$ and $k_4$ are rate parameters.

The rate of change of $u$ contains these three terms with the signs reversed. In addition, because $u$ and GEF together form the complex of concentration $m$ (which is assumed to be reversible) we get two additional terms describing this conversion. The rate of change of $u$ is therefore given by

$$\left[\frac{\partial u}{\partial t}\right]_{\text{reaction}} = k_1 vg + k_2 vm - k_3 \frac{u}{u + k_4} - k_5 ug + k_{-5} m,$$

where the term $k_5 ug$ describes the formation of complex, and the term $k_{-5} m$ is due to the reversed process, of complex being dissolved into $u$ and GEF. The two equations for $m$ and $g$ are given by

$$\left[\frac{\partial m}{\partial t}\right]_{\text{reaction}} = k_5 ug - k_{-5} m,$$
$$\left[\frac{\partial g}{\partial t}\right]_{\text{reaction}} = -k_5 ug + k_{-5} m,$$

where $k_5$ and $k_{-5}$ are rate parameters.

In order to make the model more pertinent to mathematical analysis, two assumptions are being made. The first is a quasi-steady state approximation of the complex formation:

$$\left[\frac{\partial m}{\partial t}\right]_{\text{reaction}} = 0$$
$$\Rightarrow m = \frac{k_5}{k_{-5}} ug,$$

and the second is that the total amount of GEF, either free or bound into the complex, is constant and equal to $g_0$:

$$m + g = g_0.$$

These two assumptions allows one to get rid of the differential equations for $m$ and $g$, therefore ending up with a system of the form (3.12). The resulting

function $f$ one obtains after simplifications is given by

$$f(u,v) = k_1 v g_0 \left(1 - \frac{K_5 u}{1+K_5}\right) + k_2 v \frac{K_5 u g_0}{1+K_5 u} - k_3 \frac{u}{u+k_4}, \tag{3.15}$$

where $K_5 = k_5/k_{-5}$, and the function $q$ given by (3.14).

It is now time to present our choice of model used in **Paper IV**. The choice of function $q$ is the same, with the small exception that we do not consider only the positive part of the term $(c_{max} - u - v)$ as discussed previously. To understand our modelling assumptions, a schematic representation of our model is presented in Figure 3.7.

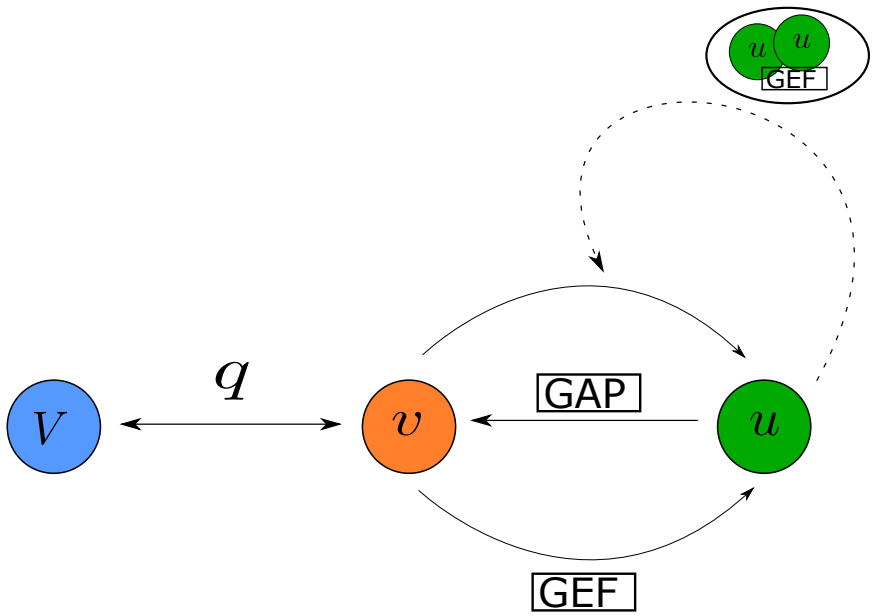


**Figure 3.7:** Schematic illustration of the interactions between $V$, $v$ and $u$ of our model presented in **Paper IV**.

We do not explicitly consider the concentrations of GEFs or GAPs, instead we make the following assumptions:

1. The activation mediated by GEF is governed by the law of mass action, and the rate is therefore proportional to $v$.

2. The inactivation mediated by GAP is governed by the law of mass action, and the rate is therefore proportional to $u$.

3. The activation can be catalyzed by a GEF-complex that binds to two GTP-bound Cdc42-molecules.

4. The complex is in quasi-steady state.

With these assumptions we obtain the reaction for $v$:

$$\left[\frac{\partial v}{\partial t}\right]_{\text{reaction}} = -k_1 v - k_2 v m + k_3 u,$$

where the first term corresponds to the activation through GEF alone, the second term corresponds to the activation mediated by the complex $m$, and the third term is due to inactivation. Similarly for $u$ we obtain

$$\left[\frac{\partial u}{\partial t}\right]_{\text{reaction}} = k_1 v + k_2 v m - k_3 u - k_4 u^2 + k_5 m$$

where the fourth term correspond to the formation of the complex, and the fifth term to the reversed process. The equation for the complex $m$ becomes

$$\left[\frac{\partial m}{\partial t}\right]_{\text{reaction}} = k_4 u^2 - k_5 m.$$

Assuming now that $[\partial m/\partial t]_{\text{reaction}} = 0$ we see that $m = u^2(k_4/k_5)$. And inserting this into the equations for $v$ and $u$ we obtain

$$\begin{aligned}\left[\frac{\partial v}{\partial t}\right]_{\text{reaction}} &= k_1 v - k_3 u - \frac{k_2 k_4}{k_5} u^2 v,\\ \left[\frac{\partial u}{\partial t}\right]_{\text{reaction}} &= -k_1 v + k_3 u + \frac{k_2 k_4}{k_5} u^2 v.\end{aligned}$$

We can see that our reaction-function $f$ is therefore given by

$$f(u, v) = -k_1 v + k_3 u + \frac{k_2 k_4}{k_5} u^2 v. \tag{3.16}$$

The main difference between our assumptions and those made in [75] is the feedback loop of the activation mediated by the complex. In the original model it was assumed that the feedback is linear, in the sense that GEF and a single molecule of GTP-bound Cdc42 forms the complex, whereas we assume that the feedback is nonlinear and requires two GTP-bound Cdc42 molecules. This type of mechanisms has been discussed in the literature [36]. Another difference is the assumption of Michaelis-Menten kinetics for the activation, which we do not make.

One of the advantages of our resulting function $f$ is that it contains fewer parameters compared to the original model [75].

# 4 Summary of papers

Below is a summary of the four appended papers.

## 4.1 Paper I

In the first paper we use the model described in Section 3.3 as a starting point, to model durotaxis. We assume that the jump rate $\lambda_i$ of an adhesion site located at position $x_i$ is a function of the local stiffness $E(x_i)$.

We assume that a cell exerts forces at the adhesion sites, and through the displacements senses the stiffness of the substrate. We investigate two different mechanisms for how the cells respond to the perceived stiffness. The first is based on the relative difference of displacements at the sites, and the second is based on the absolute difference of displacement of the sites.

For these two mechanisms we derive the population-level PDE model. In both cases the resulting PDE model takes the form of an advection-diffusion equation. When the cells sense relative differences in stiffness, the resulting advective velocity $V(x)$ is given by

$$V(x) = \frac{E'(x)}{E(x)},$$

and in the case of sensing the absolute difference in stiffness, the advective velocity is given by

$$V(x) = \frac{2E'(x)}{E^2(x)}.$$

We simulate both the stochastic model and the PDE model for a linearly increasing stiffness function and show that the stochastic simulations and PDE models agree well. Finally we choose a stiffness function in the shape of a sine-function to compare our model to a previous experiment where cells were seeded on a substrate with periodic stiffness of the same shape. We find that our model is able to reproduce the results observed in the experiment, namely that cells cluster on regions of high stiffness.

## 4.2 Paper II

In the second paper we also use the model of Section 3.3 as a starting point. We drop the notion of spatially varying lifetimes and instead investigate whether the displacements of the elastic substrate can result in durotactic motion of cells. The substrate is modelled as an elastic rod in one spatial dimension which becomes deformed as the cell exerts forces on it.

We investigate different substrate rigidities, with and without gradients. The forces generated by a cell come from the springs connecting the nucleus to the substrate. In the model of **Paper I** the cell spring coefficients are taken to be constant. In this study we allow them to be either constant, or depend on the substrate stiffness in a linear or quadratic fashion.

We find that when the cell forces do not depend on the stiffness of the substrate, no durotactic response can be observed even in the presence of a stiffness gradient. This indicates that the skewed mass distribution alone is not sufficient to explain the biased motion up the gradient. However, when the cell forces are assumed to increase with increasing stiffness, the cells migrate preferentially up the stiffness gradient.

## 4.3 Paper III

In the third paper we developed a stochastic model of glioblastoma growth in the brain of mice. The model takes the form of a biased random walk on a 3D lattice. Cells are able to proliferate and migrate between voxels. Diffusion tensor imaging data is incorporated into the model and used to guide cell migration. Each voxel is associated with a diffusion tensor, which can be used in multiple ways to derive migration rules for the cells. We use the mean diffusivity for the overall migration rate, and the principal eigenvectors to provide bias in the direction of migration.

We use numerical simulations to demonstrate different anisotropic patterns of spread that can be produced. We show how the model parameters influence total population size, as well as the invasion velocity.

To test the validity of the model we compare simulations to data obtained from mouse xenograft experiments, where cancer cells are injected into the brain of mice. We find that the model is not able to accurately reproduce the experimental data, so a number of possible extensions are discussed.

## 4.4 Paper IV

In the fourth paper we develop a model for spontaneous symmetry breaking. The model consists of a system of three reaction-diffusion equations governing the concentrations of GTP-, GDP-, and GDI-bound forms of Cdc42. The spatial domain is three-dimensional and consists of the interior of a ball (cytosol) and its surface (cell membrane). The GDI-bound form exists in the cytosol, whereas the GTP- and GDI-bound forms exist on the membrane.

The model is similar to previous models of polarization, but makes use of a new choice of reaction-function $f$ governing the activation/inactivation. We use numerical simulations of the model to demonstrate its ability to generate patterns of relevance, namely the accumulation of active Cdc42 in a single spot (pole) on the membrane.

We conduct numerical experiments to investigate how the parameters of the model influence the properties of patterns generated. We determine which parameters satisfy the criteria of classic and non-classic Turing instability, and how they influence the size of the pole, the number of poles as well as the time to polarization.

# 5 Concluding remarks

The modelling of **Papers I** and **II** together demonstrate that multiple distinct mechanisms can result in durotaxis, at least in theory. The results from the theoretical studies encourage experiments aimed at investigating how much of the observed directionality comes from reinforcements of adhesion sites, and how much comes from substrate deformations along with stiffness dependent traction forces. The work in the two papers demonstrates how relatively simple models can be used to investigate "what-if" scenarios, by isolating single possible mechanisms, and analysing the models.

As a future extension, the two models can be combined into a single model in which both the lifetimes of adhesion sites and the forces generated by the cells depend on the substrate stiffness. By obtaining the model parameters from experimental data, one could then determine how much of the observed drift is due to each mechanism, or if there is yet another mechanism that is causing the bias towards stiffer regions.

In a broader context, making progress in understanding both single and collective cell migration is of great importance in further developing cancer treatment. Cancer cells have been shown to be able to adapt their migratory strategies to different experimental conditions, and in response to drug treatment [30]. However, a class of drugs targeting cell invasion and metastasis, referred to as migrastatics [32] are being researched. They are for example aimed at disrupting the actin polymerization process or the contractile apparatus. Models such as the ones developed in this thesis can offer insights into the details of migration, and could possibly be used to investigate the effects of treatment schemes aimed at inhibiting invasion.

In order to improve cancer diagnosis and treatment further, information from individual patients can be obtained and used to guide decision making. This is referred to as personalized medicine, or precision medicine [50]. The data can come from genomics or proteomics [14], but also from medical imaging. Mathematical models of cancer which use medical imaging data in a patient-specific setting [86] now exist. As was demonstrated in our third paper, and which also can be seen in [86], there are instances where the tumor has grown in an irregular fashion that is difficult to capture with models based on random motion, even in the presence of bias. Hopefully, further developments will help in resolving the current issues and improve the predictive powers of the models even more.

# Bibliography


[1] Julius Adler. Chemotaxis in bacteria. *Annual review of biochemistry*, 44(1):341–356, 1975.

[2] Abramo Agosti, Clara Cattaneo, Chiara Giverso, Davide Ambrosi, and Pasquale Ciarletta. A computational framework for the personalized clinical treatment of glioblastoma multiforme. *ZAMM-Journal of Applied Mathematics and Mechanics/Zeitschrift für Angewandte Mathematik und Mechanik*, 98(12):2307–2327, 2018.

[3] Bruce Alberts, Alexander Johnson, Julian Lewis, Martin Raff, Keith Roberts, and Peter Walter. Molecular biology of the cell, 5th edn. garland science. *New York*, 2008.

[4] Wolgang Alt. Biased random walk models for chemotaxis and related diffusion approximations. *Journal of mathematical biology*, 9(2):147–177, 1980.

[5] Komal Anjum, Bibi Ibtesam Shagufta, Syed Qamar Abbas, Seema Patel, Ishrat Khan, Sayed Asmat Ali Shah, Najeeb Akhter, and Syed Shams ul Hassan. Current status and future therapeutic perspectives of glioblastoma multiforme (gbm) therapy: A review. *Biomedicine & Pharmacotherapy*, 92:681–689, 2017.

[6] HC Berg and DA Brown. Chemotaxis in escherichia coli analyzed by three-dimensional tracking. In *Chemotaxis: Its Biology and Biochemistry*, volume 19, pages 55–78. Karger Publishers, 1974.

[7] Ralph A Bradshaw and Edward A Dennis. *Handbook of cell signaling*. Academic press, 2009.

[8] Dennis Bray. *Cell movements: from molecules to motility*. Garland Science, 2000.

[9] Christopher JW Breward, Helen M Byrne, and Claire E Lewis. A multiphase model describing vascular tumour growth. *Bulletin of mathematical biology*, 65(4):609–640, 2003.

[10] Nicholas F Britton. *Essential mathematical biology*. Springer Science & Business Media, 2012.

[11] Joseph P Califano and Cynthia A Reinhart-King. Substrate stiffness and cell area predict cellular traction stresses in single cells and cells in contact. *Cellular and molecular bioengineering*, 3(1):68–75, 2010.

[12] Stephen B Carter. Principles of cell motility: the direction of cell movement and cancer invasion. *Nature*, 208(5016):1183–1187, 1965.

[13] Subrahmanyan Chandrasekhar. Stochastic problems in physics and astronomy. *Reviews of modern physics*, 15(1):1, 1943.

[14] Tingting Cheng and Xianquan Zhan. Pattern recognition for predictive, preventive, and personalized medicine in cancer. *EPMA Journal*, 8(1):51–60, 2017.

[15] Jian-geng Chiou, Mohan K Balasubramanian, and Daniel J Lew. Cell polarity in yeast. *Annual review of cell and developmental biology*, 33:77–101, 2017.

[16] PH Ciarletta, Thomas Hillen, Hans Othmer, and D Trucu. *Mathematical models and methods for living systems*. Springer, 2016.

[17] Edward A Codling, Michael J Plank, and Simon Benhamou. Random walk models in biology. *Journal of the Royal Society Interface*, 5(25):813–834, 2008.

[18] John Condeelis, Robert H Singer, and Jeffrey E Segall. The great escape: when cancer cells hijack the genes for chemotaxis and motility. *Annu. Rev. Cell Dev. Biol.*, 21:695–718, 2005.

[19] Davide Cusseddu, Leah Edelstein-Keshet, John A Mackenzie, Stéphanie Portet, and Anotida Madzvamuse. A coupled bulk-surface model for cell polarisation. *Journal of theoretical biology*, 481:119–135, 2019.

[20] JC Dallon, Emily J Evans, Christopher P Grant, and William V Smith. Cell speed is independent of force in a mathematical model of amoeboidal cell motion with random switching terms. *Mathematical biosciences*, 246(1):1–7, 2013.

[21] JC Dallon, Matthew Scott, and William V Smith. A force based model of individual cell migration with discrete attachment sites and random switching terms. *Journal of biomechanical engineering*, 135(7), 2013.

[22] Mauro Dorato. Mathematical biology and the existence of biological laws. In *Probabilities, Laws, and Structures*, pages 109–121. Springer, 2012.

[23] Brian J DuChez, Andrew D Doyle, Emilios K Dimitriadis, and Kenneth M Yamada. Durotaxis by human cancer cells. *Biophysical journal*, 116(4):670–683, 2019.

[24] THW Engelmann. Ueber den faserigen bau der kontraktilen substanz mit besonderer berucksichtigung der glatten und doppelt schrag gestreiften muskelfasern. *Pflügers Arch.*, 25:73–81, 1881.

[25] Jorge Escribano, Raimon Sunyer, María Teresa Sánchez, Xavier Trepat, Pere Roca-Cusachs, and José Manuel García-Aznar. A hybrid computational model for collective cell durotaxis. *Biomechanics and modeling in mechanobiology*, 17(4):1037–1052, 2018.

[26] Morteza Esmaeili, Anne Line Stensjøen, Erik Magnus Berntsen, Ole Solheim, and Ingerid Reinertsen. The direction of tumour growth in glioblastoma patients. *Scientific reports*, 8(1):1–6, 2018.

[27] Sandrine Etienne-Manneville. Cdc42-the centre of polarity. *Journal of cell science*, 117(8):1291–1300, 2004.

[28] Birte U Forstmann, Eric-Jan Wagenmakers, et al. *An introduction to model-based cognitive neuroscience*. Springer, 2015.

[29] Christian Frantz, Kathleen M Stewart, and Valerie M Weaver. The extracellular matrix at a glance. *Journal of cell science*, 123(24):4195–4200, 2010.

[30] Peter Friedl and Katarina Wolf. Tumour-cell invasion and migration: diversity and escape mechanisms. *Nature reviews cancer*, 3(5):362–374, 2003.

[31] Sabato Fusco, Valeria Panzetta, and Paolo A Netti. Mechanosensing of substrate stiffness regulates focal adhesions dynamics in cell. *Meccanica*, 52(14):3389–3398, 2017.

[32] Aneta Gandalovičová, Daniel Rosel, Michael Fernandes, Pavel Veselỳ, Petr Heneberg, Vladimír Čermák, Luboš Petruželka, Sunil Kumar, Victoria Sanz-Moreno, and Jan Brábek. Migrastatics—anti-metastatic and anti-invasion drugs: promises and challenges. *Trends in cancer*, 3(6):391–406, 2017.

[33] Benjamin Geiger, Joachim P Spatz, and Alexander D Bershadsky. Environmental sensing through focal adhesions. *Nature reviews Molecular cell biology*, 10(1):21–33, 2009.

[34] A Giese, R Bjerkvig, ME Berens, and M Westphal. Cost of migration: invasion of malignant gliomas and implications for treatment. *Journal of clinical oncology*, 21(8):1624–1636, 2003.

[35] Sidney Goldstein. On diffusion by discontinuous movements, and on the telegraph equation. *The Quarterly Journal of Mechanics and Applied Mathematics*, 4(2):129–156, 1951.

[36] Andrew B Goryachev and Marcin Leda. Many roads to symmetry breaking: molecular mechanisms and theoretical models of yeast cell polarity. *Molecular biology of the cell*, 28(3):370–380, 2017.

[37] Andrew B Goryachev and Alexandra V Pokhilko. Dynamics of cdc42 network embodies a turing-type mechanism of yeast cell polarity. *FEBS letters*, 582(10):1437–1443, 2008.

[38] Mukund Gupta, Bryant Doss, Chwee Teck Lim, Raphael Voituriez, and Benoit Ladoux. Single cell rigidity sensing: a complex relationship between focal adhesion dynamics and large-scale actin cytoskeleton remodeling. *Cell adhesion & migration*, 10(5):554–567, 2016.

[39] Sangyoon J Han, Kevin S Bielawski, Lucas H Ting, Marita L Rodriguez, and Nathan J Sniadecki. Decoupling substrate stiffness, spread area, and micropost density: a close spatial relationship between traction forces and focal adhesions. *Biophysical journal*, 103(4):640–648, 2012.

[40] Archibald Vivian Hill. The diffusion of oxygen and lactic acid through tissues. *Proceedings of the Royal Society of London. Series B, Containing Papers of a Biological Character*, 104(728):39–96, 1928.

[41] Eric C Holland. Glioblastoma multiforme: the terminator. *Proceedings of the National Academy of Sciences*, 97(12):6242–6244, 2000.

[42] ME Hubbard and HM Byrne. Multiphase modelling of vascular tumour growth in two spatial dimensions. *Journal of theoretical biology*, 316:70–89, 2013.

[43] Anna Huttenlocher. Cell polarization mechanisms during directed cell migration. *Nature cell biology*, 7(4):336–337, 2005.

[44] Brett C Isenberg, Paul A DiMilla, Matthew Walker, Sooyoung Kim, and Joyce Y Wong. Vascular smooth muscle cell durotaxis depends on substrate stiffness gradient strength. *Biophysical journal*, 97(5):1313–1322, 2009.

[45] Saâd Jbabdi, Emmanuel Mandonnet, Hugues Duffau, Laurent Capelle, Kristin Rae Swanson, Mélanie Pélégrini-Issac, Rémy Guillevin, and Habib Benali. Simulation of anisotropic growth of low-grade gliomas using diffusion tensor imaging. *Magnetic Resonance in Medicine: An Official Journal of the International Society for Magnetic Resonance in Medicine*, 54(3):616–624, 2005.

[46] Alexandra Jilkine and Leah Edelstein-Keshet. A comparison of mathematical models for polarization of single eukaryotic cells in response to guided cues. *PLoS Comput Biol*, 7(4):e1001121, 2011.

[47] Danielle Joaquin, Michael Grigola, Gubeum Kwon, Christopher Blasius, Yutao Han, Daniel Perlitz, Jing Jiang, Yvonne Ziegler, Ann Nardulli, and K Jimmy Hsia. Cell migration and organization in three-dimensional in vitro culture driven by stiffness gradient. *Biotechnology and bioengineering*, 113(11):2496–2506, 2016.

[48] Jayme M Johnson, Meng Jin, and Daniel J Lew. Symmetry breaking and the establishment of cell polarity in budding yeast. *Current opinion in genetics & development*, 21(6):740–746, 2011.

[49] William Ogilvy Kermack and Anderson G McKendrick. A contribution to the mathematical theory of epidemics. *Proceedings of the royal society of*

*london. Series A, Containing papers of a mathematical and physical character*, 115(772):700–721, 1927.

[50] Fatemeh Khatami, Bagher Larijani, Shekoufeh Nikfar, Mandana Hasanzad, Kiarad Fendereski, and Seyed Mohammad Tavangar. Personalized treatment options for thyroid cancer: current perspectives. *Pharmacogenomics and personalized medicine*, 12:235, 2019.

[51] Min-Cheol Kim, Yaron R Silberberg, Rohan Abeyaratne, Roger D Kamm, and H Harry Asada. Computational modeling of three-dimensional ecm-rigidity sensing to guide directed cell migration. *Proceedings of the National Academy of Sciences*, 115(3):E390–E399, 2018.

[52] Marcin Kotulski. Asymptotic distributions of continuous-time random walks: a probabilistic approach. *Journal of statistical physics*, 81(3-4):777–792, 1995.

[53] Satoshi Kurosaka and Anna Kashina. Cell biology of embryonic migration. *Birth Defects Research Part C: Embryo Today: Reviews*, 84(2):102–122, 2008.

[54] Ryszard Kutner and Jaume Masoliver. The continuous time random walk, still trendy: fifty-year history, state of art and outlook. *The European Physical Journal B*, 90(3):50, 2017.

[55] Caterina AM La Porta and Stefano Zapperi. *Cell Migrations: Causes and Functions*, volume 1146. Springer, 2019.

[56] Douglas A Lauffenburger and Alan F Horwitz. Cell migration: a physically integrated molecular process. *Cell*, 84(3):359–369, 1996.

[57] Fong Yin Lim, Yen Ling Koon, and Keng-Hwee Chiam. A computational model of amoeboid cell migration. *Computer methods in biomechanics and biomedical engineering*, 16(10):1085–1095, 2013.

[58] Chun-Min Lo, Hong-Bei Wang, Micah Dembo, and Yu-li Wang. Cell movement is guided by the rigidity of the substrate. *Biophysical journal*, 79(1):144–152, 2000.

[59] Athanasius FM Marée, Verônica A Grieneisen, and Paulien Hogeweg. The cellular potts model and biophysical properties of cells, tissues and morphogenesis. In *Single-cell-based models in biology and medicine*, pages 107–136. Springer, 2007.

[60] Sophie G Martin. Spontaneous cell polarization: Feedback control of cdc42 gtpase breaks cellular symmetry. *Bioessays*, 37(11):1193–1201, 2015.

[61] William V Mayneord. On a law of growth of jensen's rat sarcoma. *The American Journal of Cancer*, 16(4):841–846, 1932.

[62] Ralf Metzler and Joseph Klafter. The random walk's guide to anomalous diffusion: a fractional dynamics approach. *Physics reports*, 339(1):1–77, 2000.

[63] Elliott W Montroll and George H Weiss. Random walks on lattices. ii. *Journal of Mathematical Physics*, 6(2):167–181, 1965.

[64] Yoichiro Mori, Alexandra Jilkine, and Leah Edelstein-Keshet. Wave-pinning and cell polarity from a bistable reaction-diffusion system. *Biophysical journal*, 94(9):3684–3697, 2008.

[65] JD Murray. *Mathematical biology II: spatial models and biomedical applications*, volume 3. Springer-Verlag, 2001.

[66] Hans G Othmer, Steven R Dunbar, and Wolfgang Alt. Models of dispersal in biological systems. *Journal of mathematical biology*, 26(3):263–298, 1988.

[67] Hans G Othmer and Thomas Hillen. The diffusion limit of transport equations derived from velocity-jump processes. *SIAM Journal on Applied Mathematics*, 61(3):751–775, 2000.

[68] Mikiya Otsuji, Shuji Ishihara, Kozo Kaibuchi, Atsushi Mochizuki, Shinya Kuroda, et al. A mass conserved reaction–diffusion system captures properties of cell polarity. *PLoS Comput Biol*, 3(6):e108, 2007.

[69] Madeleine J Oudin, Oliver Jonas, Tatsiana Kosciuk, Liliane C Broye, Bruna C Guido, Jeff Wyckoff, Daisy Riquelme, John M Lamar, Sreeja B Asokan, Charlie Whittaker, et al. Tumor cell–driven extracellular matrix remodeling drives haptotaxis during metastatic progression. *Cancer discovery*, 6(5):516–531, 2016.

[70] KJ Painter and Thomas Hillen. Mathematical modelling of glioma growth: the use of diffusion tensor imaging (dti) data to predict the anisotropic pathways of cancer invasion. *Journal of theoretical biology*, 323:25–39, 2013.

[71] Clifford S Patlak. Random walk with persistence and external bias. *The bulletin of mathematical biophysics*, 15(3):311–338, 1953.

[72] Wilhelm Pfeffer. Uber chemotaktische bewegungen von bacterien, flagellaten und volvocineen. *Untersuch. Bot. Inst. Tubingen*, 2:582–661, 1888.

[73] Sergey V Plotnikov and Clare M Waterman. Guiding cell migration by tugging. *Current opinion in cell biology*, 25(5):619–626, 2013.

[74] Andreas Rätz. Turing-type instabilities in bulk–surface reaction–diffusion systems. *Journal of Computational and Applied Mathematics*, 289:142–152, 2015.

[75] Andreas Rätz and Matthias Röger. Turing instabilities in a mathematical model for signaling networks. *Journal of mathematical biology*, 65(6-7):1215–1244, 2012.

[76] Andreas Rätz and Matthias Röger. Symmetry breaking in a bulk–surface reaction–diffusion model for signalling networks. *Nonlinearity*, 27(8):1805, 2014.

[77] Michael C Reed. Why is mathematical biology so hard. *Notices of the AMS*, 51(3):338–342, 2004.

[78] Anne J Ridley, Martin A Schwartz, Keith Burridge, Richard A Firtel, Mark H Ginsberg, Gary Borisy, J Thomas Parsons, and Alan Rick Horwitz. Cell migration: integrating signals from front to back. *Science*, 302(5651):1704–1709, 2003.

[79] Wajeeh Saadi, Shur-Jen Wang, Francis Lin, and Noo Li Jeon. A parallel-gradient microfluidic chamber for quantitative analysis of breast cancer cell chemotaxis. *Biomedical microdevices*, 8(2):109–118, 2006.

[80] Alexandre Saez, Axel Buguin, Pascal Silberzan, and Benoît Ladoux. Is the mechanical activity of epithelial cells controlled by deformations or forces? *Biophysical journal*, 89(6):L52–L54, 2005.

[81] Ingmar Schoen, Beth L Pruitt, and Viola Vogel. The yin-yang of rigidity sensing: how forces and mechanical properties regulate the cellular response to materials. *Annual Review of Materials Research*, 43:589–618, 2013.

[82] Marco Scianna and Luigi Preziosi. Multiscale developments of the cellular potts model. *Multiscale Modeling & Simulation*, 10(2):342–382, 2012.

[83] Long Shi, Zuguo Yu, Zhi Mao, and Aiguo Xiao. A directed continuous time random walk model with jump length depending on waiting time. *The Scientific World Journal*, 2014, 2014.

[84] Matthew J Simpson and Ruth E Baker. Corrected mean-field models for spatially dependent advection-diffusion-reaction phenomena. *Physical Review E*, 83(5):051922, 2011.

[85] Andrew M Stein, Tim Demuth, David Mobley, Michael Berens, and Leonard M Sander. A mathematical model of glioblastoma tumor spheroid invasion in a three-dimensional in vitro experiment. *Biophysical journal*, 92(1):356–365, 2007.

[86] Amanda Swan, Thomas Hillen, John C Bowman, and Albert D Murtha. A patient-specific anisotropic diffusion model for brain tumour spread. *Bulletin of mathematical biology*, 80(5):1259–1291, 2018.

[87] Kristin R Swanson, Ellsworth C Alvord Jr, and JD Murray. A quantitative model for differential motility of gliomas in grey and white matter. *Cell proliferation*, 33(5):317–329, 2000.

[88] András Szabó and Roeland MH Merks. Cellular potts modeling of tumor growth, tumor invasion, and tumor evolution. *Frontiers in oncology*, 3:87, 2013.

[89] Diego Torrejon and Maria Emelianenko. Generalized master equations for random walks with time-dependent jump sizes. *SIAM Journal on Applied Mathematics*, 78(3):1330–1349, 2018.

[90] Katrina K Treloar, Matthew J Simpson, and Scott W McCue. Velocity-jump models with crowding effects. *Physical Review E*, 84(6):061920, 2011.

[91] Katrina K Treloar, Matthew J Simpson, and Scott W McCue. Velocity-jump processes with proliferation. *Journal of Physics A: Mathematical and Theoretical*, 46(1):015003, 2012.

[92] Theresa A Ulrich, Elena M de Juan Pardo, and Sanjay Kumar. The mechanical rigidity of the extracellular matrix regulates the structure, motility, and proliferation of glioma cells. *Cancer research*, 69(10):4167–4174, 2009.

[93] Ludovic G Vincent, Yu Suk Choi, Baldomero Alonso-Latorre, Juan C Del Álamo, and Adam J Engler. Mesenchymal stem cell durotaxis depends on substrate stiffness gradient strength. *Biotechnology journal*, 8(4):472–484, 2013.

[94] George H Wadhams and Judith P Armitage. Making sense of it all: bacterial chemotaxis. *Nature reviews Molecular cell biology*, 5(12):1024–1037, 2004.

[95] Roland Wedlich-Soldner, Steve Altschuler, Lani Wu, and Rong Li. Spontaneous cell polarization through actomyosin-based delivery of the cdc42 gtpase. *Science*, 299(5610):1231–1235, 2003.

[96] Henry C Wong and William C Tang. Finite element analysis of the effects of focal adhesion mechanical properties and substrate stiffness on cell migration. *Journal of biomechanics*, 44(6):1046–1050, 2011.

[97] Muhammad H Zaman, Roger D Kamm, Paul Matsudaira, and Douglas A Lauffenburger. Computational model for cell migration in three-dimensional matrices. *Biophysical journal*, 89(2):1389–1397, 2005.